GREEN SYNTHESIS OF COPPER OXIDE NANOPARTICLES FROM PUMPKIN (*Cucurbita maxima)* DYE EXTRACT: A PLATINUM FREE COUNTER ELECTRODE FOR DYE SENSITIZED SOLAR CELLS

BY

TENYWA STEPHEN

20/U/GMSP/13320/PD

A DISSERTATION SUBMITTED TO THE DIRECTORATE OF RESEARCH AND GRADUATE TRAINING IN PARTIAL FULFILMENT OF THE REQUIREMENTS FOR THE AWARD OF THE DEGREE OF

MASTER OF SCIENCE IN PHYSICS OF

KYAMBOGO UNIVERSITY

FEBRUARY, 2024

DECLARATION

I TENYWA STEPHEN do here by declare that this work is my original work and it has never been presented to any University or other Higher Education Institution for consideration of any similar award.

Signature: ……. Date: …….

APPROVAL

This serves as a proof that this dissertation entitled "Green synthesis of Copper oxide nanoparticles from *Cucurbita maxima* dye extract: A platinum free counter electrode for dye sensitized solar cells" was developed by Mr. TENYWA STEPHEN and has been under our supervision and now duly approved for submission to the Directorate of Research & Graduate Training, and Senate of Kyambogo University.

1. Dr. Emma Panzi Mukhokosi

   Department of Physics, Kyambogo University, Kampala Uganda

   Signature: ……. Date: ……

2. Dr. Jude Tadeo Inyalot

   Department of Chemistry, Kyambogo University, Kampala, Uganda

   Signature…… Date……

DEDICATION

This scholarly writing is dedicated to my sister Ntono Iren for her continued support and good spirit she has exhibited to me in this academic journey specially at this level. May the good Lord greatly bless her.

ACKNOWLEDGEMENT

I exalt God the Almighty for the gift of life, love, favour, wisdom as well as understanding that have enabled me complete this dissertation.

I owe much debt to my principal supervisor, Dr. Emma Panzi Mukhokosi and the co-supervisor, Dr. Jude Tadeo Inyalot for their dedication, cooperation and continuous guidance each time I contacted them throughout the various stages of development of this dissertation.

I owe profound gratitude to all my other lecturers in the Physics Department of Kyambogo University. These include; Prof. Obwoya Kinyera Sam, Prof. Eric Mucunguzi, Dr. Michael Okullo, Dr. Patrick Oyirwoth Abedigamba, Dr. Farooq Kyeyune, Mr. Enjiku Ben for their academic guidance, moral support and imparting knowledge in me.

I am obliged to thank my course mates; Tumwizire Nelson and Etindu Lawrence for the great assistance and contribution during the course of study.

My sincere thanks also go to the laboratory technicians, Mr. Kawuki Joseph, Mr. Balimunsahe John and Mr. Isabirye Isaac in the Kyambogo University Physics department and Biolology departments respectively for their time and support rendered to me all through my research work.

Lastly, I thank my sister Dr. Stella Nabirye for Moral, spiritual and medical support together with my friends, Sekitoleko Rogers, Waiswa Isaac and all those who contributed to this success in one way or another.

TABLE OF CONTENTS

LIST OF TABLES

LIST OF FIGURES

ABSTRACT

Energy is a very critical requirement for all nations that boosts economic growth and development. Dye-sensitized solar cells (DSSCs), the 3rd generation photovoltaic technology which imitate the process of photosynthesis in green plants have of recent gained overwhelming attention in solar harnessing because of their simple structure, affordable cost, simple fabrication technique, little toxicity, and comparatively high efficiency of energy conversion. Currently, Platinum is used as a counter electrode for DSSCs. However, the scarcity and high cost of Pt is still a challenge. In this study, copper oxide (CuO) nanoparticles (NPs) were synthesized using *Cucurbita maxima* plant leaf dye extract and applied as an electrocatalytic CE in DSSCs. The CuO NPs were characterized using XRD, TEM, UV-Visible spectrophotometer and FTIR to obtain their crystal structure, surface morphology, optical properties and chemical bonds respectively. Three individual natural dyes from pumpkin leaves (P), sweet potato leaves (S) and hibiscus flowers (H), along with their composites, P:H and S:H in varying ratios were extracted, their optical properties studied and used as photosensitizers. The results indicate that the fabricated DSSC with P:H-1:3 composite dyes yielded the highest PCE of 8.7×10^{-4} %, a short circuit current density (J_{sc}) of 13.94 μA/cm^2 and an open circuit voltage (V_{oc}) of 0.29 V compared to S:H-1:3 composite and individual dyes under one-sun illumination from a solar simulator (AM1.5 100 mWcm^{-2}).

CHAPTER ONE: INTRODUCTION

1.1 Background of the study

Energy is a very critical requirement for all nations that boosts economic growth and development. Promoting the use of energy is vital so as to realize the United Nations Sustainable Development Goals, SDGs (Pueyo and Maestre, 2019). Gielen et al, highlighted that "the share of renewable energy in the overall primary energy supply is projected to grow from 15 % in 2015 to 63 % by 2050." (Gielen et al., 2019). There are various sources of renewable energy; these include solar, wind, hydropower, biomass and geothermal energy. Among the renewable energy forms, solar energy has attracted much attention from researchers due to its benefits as compared to the other alternative forms. Solar energy is clean energy source and does not generate greenhouse gases, it is readily available and at no cost except the cost of fabricating the solar cells. Ali et al stipulated that, annually the market share for photovoltaic (PV) modules exponentially increased between the years 2000 and 2015. In this time it was anticipated that the rising trend would persist for the coming few years (Ali et al., 2016). Up to date, wafer-based crystalline silicon which are the first-generation solar cells are still dominating the market. The greatest challenge is that purification of silicon requires too much energy which has resulted into high module prices. As a solution to the high cost of PV cells, new technologies have emerged including thin film solar cells in the second-generation PV technology. Among others in this category are the CuIn-$GaSe_2$, CdTe (Repins et al., 2008) and perovskite solar cells that have of late attained the highest power conversion efficiency (PCE) of 23.3% with a single-junction layout (Mora-Seró et al., 2020). Today, dye sensitized solar cells (DSSCs) is another category in the third-generation of photovoltaic devices which are extensively being researched as prospective solar cells since they have simple structure, affordable fabrication technique, little toxicity, and relatively high efficiency of energy conversion (O'regan and Grätzel, 1991). Over time, the PCE of DSSCs has steadily been

enhanced with a currently reported efficiency of 14.7 % which was obtained with collaborative sensitization of silyl-anchor and carboxy-anchor dyes (Kakiage et al., 2015). However, additional cost reduction for DSSCs is necessary together with the need to further improve the current efficiency (Kay and Grätzel, 1996, Ito et al., 2006). The primary components of DSSCs include the sensitizer (dye), photo-anode (working electrode), counter electrode (CE) and electrolyte. Platinum (Pt) is currently the conventional CE being used in DSSCs given its outstanding properties that include; high conductivity to electricity, outstanding catalytic activity and excellent chemical stability towards reduction of I_3^- and has proven to be a successful material for producing high-performance DSSCs (Zhou et al., 2008, Papageorgiou et al., 1997). However, the scarcity and high cost of Pt makes its widespread use impractical. For this reason, researchers have continued to search for alternative CE materials. Various alternative CEs have been fabricated by a number of researchers to substitute the conventional expensive Pt. However, these alternatives must be affordable and should have all platinum-level performance characteristics for DSSCs application in order to achieve the purpose. Among the fabricated alternatives include; metal composites (Li et al., 2015), nitrides (Xu et al., 2012), carbides (Cai et al., 2017), oxides (Yun et al., 2012), conducting polymers (Yohannes and Inganäs, 1998, Xiao et al., 2014), pure transitional metal elements like ruthenium (An et al., 2016) and silver (Snaith et al., 2007), carbon related materials such as; graphene (Kim et al., 2018), carbon black (Cao et al., 2017), carbon-nanotubes (Chen et al., 2016) and graphite (Li et al., 2015), carbon black (Murakami et al., 2006, Wu et al., 2016), metal sulfides (Zhao et al., 2013, Song et al., 2016, Rao et al., 2014) and metal oxides(Yun et al., 2012, Shashanka et al., 2020).

Among the oxides is copper oxide (CuO), a p-type semiconductor with a low bandgap (E_g 1.2 eV in bulk) has received a lot of research attention due to its superb electrical, conductivity, catalytic and antibacterial properties (Vijaya Kumar et al., 2001, Abboud et al., 2014). CuO is

an excellent material that has a number of applications like in gas sensors, superconductors, batteries, catalysis, solar energy conversion, field emission emitters, large magnet resistance material and photovoltaic devices (Gao et al., 2013, Zheng et al., 2000, Yang et al., 2013). However, most production methods for CuO are expensive. In an effort to find an alternatively cheaper CE material for use in DSSCs, green synthesis of CuO NPs has been considered as one of the best and cheapest options (Parveen et al., 2016). For instance; Sharma et al, synthesized CuO NPs from leaf extract of *Calotropis gigantea* by green method from which they fabricated a CE for DSSCs. A fill factor (FF) of 0.62 along with high short circuit current density of 8.13 mA/cm^2, fairly high solar to electrical energy conversion efficiency of 3.4 %, and an open circuit voltage of 0.676 V were obtained (Sharma et al., 2015). However, further research on green synthesis of CuO NPs from other plant leaves need to done to further improve on the particle size and overall efficiency for DSSCs solar cell application.

In this dissertation, CuO NPs were for the first time synthesized using *Cucurbita maxima* leaf extract as a reducing/chelating agent of Copper (II) nitrate (Cu $(NO_3)_2$) salt to CuO NPs. Uniformly synthesized CuO NPs were characterized with XRD, TEM, UV-Visible spectrophotometer and FTIR. Using natural dye solutions from pumpkin leaves, sweet potato leaves and hibiscus flowers as a photon absorber, the DSSC based on CuO NPs with P:H-1:3 composite dyes exhibited the highest *PCE* of 8.7×10^{-4} % under one-sun illumination.

1.2 Statement of the problem

In DSSCs, the counter electrode (CE) is a very fundamental and necessary component in the general functioning of the cell. The CE is regarded to be a crucial component because of its relevance of enabling electron exchange by collecting electrons from the external circuit to catalyze the redox pair in the electrolyte. Currently, platinum (Pt) is used as the CE in DSSCs given its excellent conductivity to electricity, outstanding catalytic reduction ability and chemical stability (Zhou et al., 2008). However, Pt is scarce and expensive and hence the need

for an alternative CE to be used in DSSCs. In this study, low cost CuO NPs were synthesized by green method and used as a DSSC CE.

1.3 General objective of the study

To synthesize copper oxide nanoparticles using *Cucurbita maxima* dye extract for application as a counter electrode for dye sensitized solar cells.

1.4 Specific objectives of the study

To succeed in achieving the above major objective, the specific objectives were:

(i) To determine the crystal structure, particle size and surface morphology of CuO nanoparticle.

(ii) To investigate the optical properties and identify chemical bonds in CuO nanoparticles.

(iii) To determine optical absorption properties of dyes extracted from hibiscus flower, sweet potato leaves, pumpkin leaves and their composites.

(iv) To determine the power conversion efficiency of the DSSC using CuO NPs as a CE.

1.5 Scope of the study

This study put focus on counter electrode fabricated using copper oxide as platinum free CE. The experiments were carried out in the Physics Laboratories of Kyambogo University and Ithemba Labs, South Africa.

1.6 Significance of the study

The research findings will enable the solar cell manufacturers to choose appropriate, relatively cheaper and abundantly available materials in which CE can be made when fabricating DSSCs for commercial and large-scale purposes. This will make the solar cells cheaper for the final buyer/user.

This research will be useful in realizing the United Nations Sustainable Development Goals (SDGs) number 7 and 13. Furthermore, the research addresses Uganda's vision 2040, that is, vision targets 14 and 15 (Pueyo and Maestre, 2019, Balyejjusa, 2015).

Lastly, the information from this study will be used by other researchers to do additional and related research.

CHAPTER TWO: LITERATURE REVIEW

2.1 Introduction

The literature review provides the conceptual and theoretical support to this research based on prior knowledge. It attempts to review the related literature about solar cell, DSSC, theory and methods on nanoparticle and thin film preparation used in this research, Current-Voltage (*I-V)* measurement and the various characterization methods in this research.

2.2 Solar cell

A solar cell is also referred to as a photovoltaic (PV) cell. Photovoltaic means converting light (photons) to electricity (voltage) and this process is termed as photovoltaic effect. A solar cell is an electrical device which converts light energy into electricity by means of photovoltaic effect (Pandikumar et al., 2019).

To boost the amount of electricity generated, solar cells are arranged to form a module, which can be arranged to form an array as shown in Figure 2.1.

Figure 2.1: Illustration of (a) a solar cell (b) solar panel/module and (c) solar array. Reproduced with permission (Khaled et al., 2020).

Energy conversion in solar cells mainly takes two main steps. Initially, light absorption generates an electron-hole pair. Secondly, the design of the device separates the electron and hole, sending the former to the negative terminal and then the latter to the positive terminal, and as a result, electrical power is produced (Markvart and Castañer, 2018).

2.3 Dye sensitized solar cell (DSSC)

Kalyanasundaram (2010), defines a DSSC as a thin-layered solar cell made up of two transparent conducting oxide (TCO) electrodes sandwiched onto one another (Kalyanasundaram, 2010). These two TCO electrodes are; the photo-anode which is usually made of titanium dioxide (TiO_2) semi-conducting nanoparticles with adsorbed sensitizer (dye). In this case, the dyes normally used are ruthenium (Ru) complexes which act as photon absorbers. The other electrode is the counter electrode (CE), normally platinum (Pt). However numerous research is being done in the areas of photo-anode, counter electrode and sensitizer (dye) trying to come up with some other substitutes for these materials.

The evolution of DSSCs started in the year 1972 using chlorophyll as sensitized zinc oxide (ZnO) electrode solar cell (Tributsch, 1972). With the dye acting as chlorophyll, the DSSCs working principle can be linked to the process of photosynthesis in plants (Mingsukang et al., 2017). Just like any other solar cell, DSSC works by illuminating it with photon energy. Electrons leave the semiconducting network layer to facilitate electron transfer to the external circuit. This process is completed after the redox mediator in the charge transfer medium brings them back to the sensitizers. Figure 2.2 shows the structure and working of the DSSC.

2.3.1 Working principle of DSSC

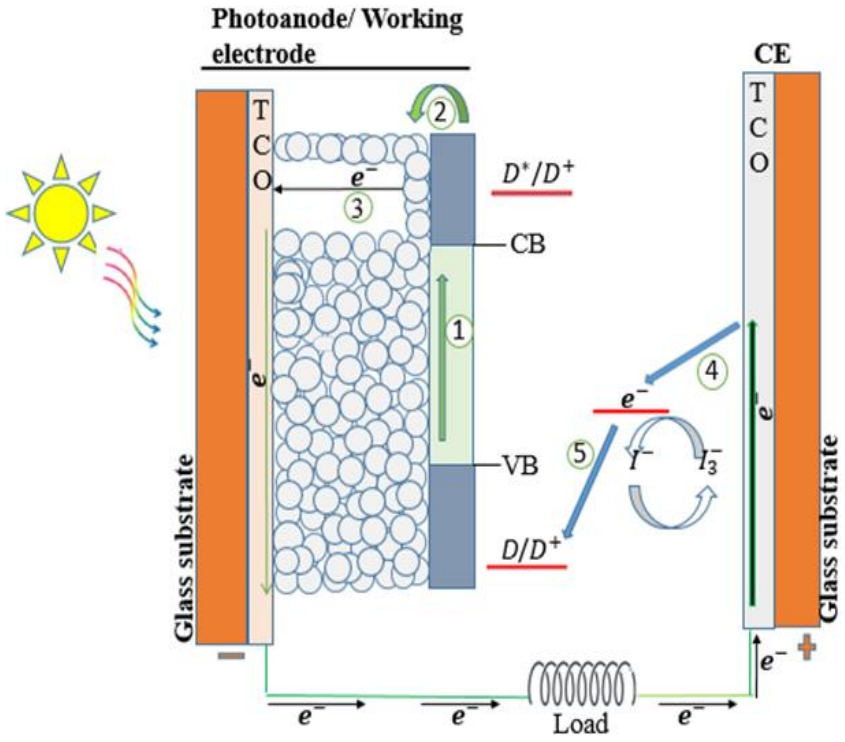

Figure 2.2: Diagram showing the parts of a DSSC and its operation.

The internal processes that take place inside the DSSC (Figure 2.2) are explained as follows.

Absorption of photons by the sensitizer (dye molecules); Initially, in the absence of photon energy (solar radiation), the dye molecule (sensitizer) is in its ground state (D).

When the Solar cell is irradiated with photon energy, the molecules in the dye absorb the photons and produce photo-excited electrons. At this level, the dye molecule overcomes the band gap and changes to a photo excited state, D^*.

$D + h\nu \rightarrow D^*$ ……..……..……..…… 2.1

Oxidation of the dye molecules; The excited dye then undergoes oxidation as it injects electrons into the conduction band (CB) of the semi-conductor (TiO_2). Here, electrons travel from the photoanode through an external loop to the transparent conducting oxide glass substrate via a thin layer of porous TiO_2, thereby creating current and completing the circuit.

$$D^{*} \rightarrow D^{+}_{absorption\ of\ TiO_2} + e^{-}_{injected} \quad \text{2.2}$$

Electron diffusion; The injected electrons travel via the semiconducting network to the rear contact where they are reduced onto the counter electrode by passing via the load and counter electrode.

$$I_3^{-} + 2e^{-}_{absorption\ of\ TiO_2} \rightarrow 3I^{-}_{absorptio\ of\ TiO_2} \quad \text{2.3}$$

Regeneration of the sensitizer (dye); The injected electrons are transferred between the photo-anode conducting material (TiO_2) where they are extracted and given as electrical energy to the load. The redox pairs in the electrolyte, that is, the iodide and triiodide ($I^{-}$and I_3^{-}) redox pairs give the oxidized-sensitizer electrons and hence making it to regenerate.

$$D^{+}_{absorption} + \frac{3}{2} I_3^{-} \rightarrow D_{absorption\ of\ TiO_2} + \frac{1}{2} I_3^{-} \quad \text{2.4}$$

Regeneration of the redox mediator; Finally, the iodide and the redox mediator in the electrolyte move to the CE, which is the cathode where it gets regenerated by reducing tri-iodide to iodide.

$$I_3^{-} + 2.e^{-}_{absorption\ if\ TiO_2} \rightarrow 3I^{-}_{anod} + h\nu \quad \text{2.5}$$

To achieve photo-electric conversion, a continuous cycle (2.1) to (2.5) has to be kept constant by illumination of the solar cell device such that it maintains a photovoltaic system with regenerative and steady energy conversion (Nazeeruddin et al., 2011, Halme et al., 2010, Mingsukang et al., 2017).

2.4 General overview of nanoparticle preparation method used in this study

2.4.1 Green synthesis method

According to Kumari et al (2021), green synthesis of nanomaterials means the synthesis of various nanoparticles from different bioactive agents including materials of plant, micro-

organisms, and several biowastes such as wastes from fruit peelings, wastes of vegetable, agricultural waste, shell of egg, etc. (Kumari et al., 2021). It is therefore a bottom-up strategy in which NPs are created when organic molecules originating from biological resources, oxidize or undergo reduction of metallic ions. The green synthesis of metallic nanoparticles has recently become an area of focus in research. “Green synthesis" is used, to mean a cheap and straightforward procedure that does not involve the use of high cost or complicated equipment (Britto-Hurtado and Cortez-Valadez, 2022). This method has got numerous advantages as compared to other methods of preparing nanoparticles. The following are some of the of the advantages;

(i) Easy to customize size, shape and nature by adjusting pH, temperature and nutrient media.

(ii) Reduces health hazards to researchers, that is, toxic chemical concentrations are minimized.

(iii) Environmentally friendly since bioactive agents such as plant materials are mainly used in synthesis of nanoparticles.

(iv) Economically viable since the plant materials that are mainly used are locally available at relatively no cost.

(v) Finally, the method is a straight forward one and produces stable nanoparticles quickly.

2.5 General overview of the thin film preparation method used in this study

2.5.1 Spin coating

Spin coating is a technique that involves application of regular thin films to flat substrates. Conventional steps consists of putting a little puddle of fluid resin in the middle of a substrate and spinning it at an elevated speeds, usually around 3000 rpm (Mitzi et al., 2004).

The resins spread to and finally over the substrate edges as a result of centrifugal force, leaving a thin coating of the resin on top. The viscosity of the solution coating and the rotation speed determines the thickness of the film. Four procedures are followed when using spin coating technique and these include; deposition, spin up, spin-off, and evaporation as seen in Figure 2.3.

At the start, the resin fluid to make a film is deposited on the substrate surface which is then put on the shuck that rotates it. The spin-up and spin-off stages occur such that each follows another, whereas the evaporation step occurs continuously. The spread of the deposited material or resin is done by the centrifugal force and the more the speed, the thinner and more efficient the coating film becomes. The advantages of spin coating in depositing films on substrates include; production of extremely fine, thin, and uniformly distributed coating. However the challenge is the difficulty with samples that have large area (Mishra et al., 2019).

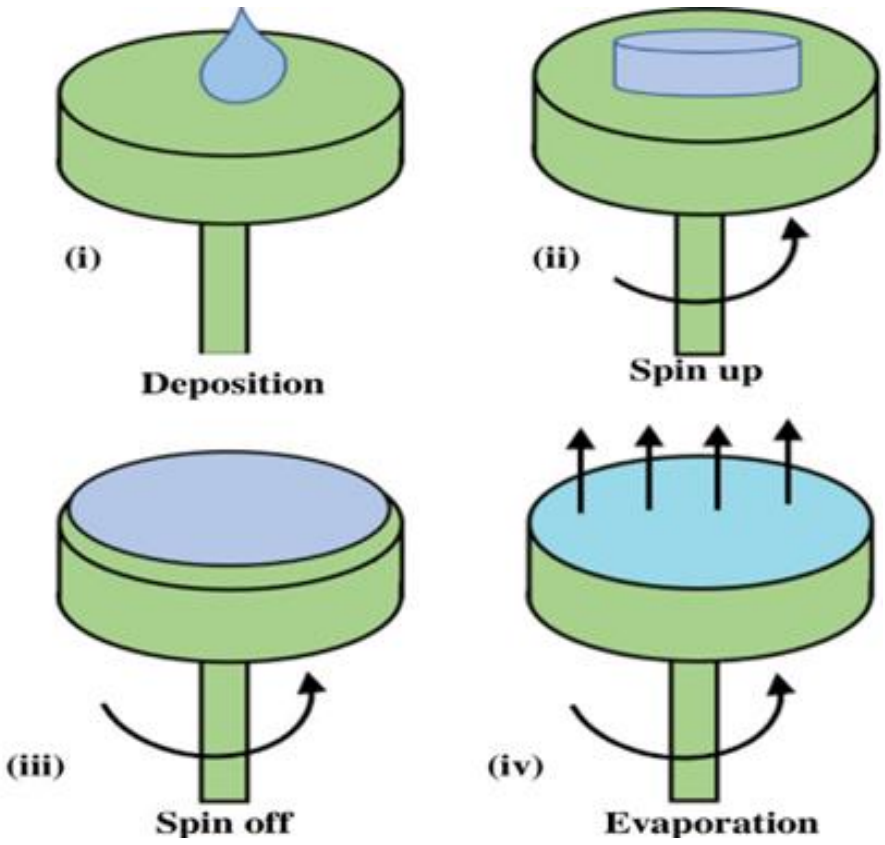

Figure 2.3: Schematic diagram of spin coating stages. Used with permission (Yilbas et al., 2019).

2.6 Theory of some of the characterization techniques in material science

2.6.1 X-ray diffraction (XRD)

This is a powerful and popular tool used for identifying the crystal structure where the crystalline atoms make an incident X-ray beam to diffract in multiple distinct directions. X-ray diffraction was proved to be a non-destructive technique and it is applied in characterization of films, NPs and structures of devices. This is done with the main intention of studying the internal structure of many materials (Moram and Vickers, 2009). When X-rays interaction with the atoms in the sample under test, a diffraction pattern is formed on the screen.

XRD pattern is helpful in obtaining numerous information about the crystal which include; the crystal structure, mean position of the atoms, their disorder and other information about

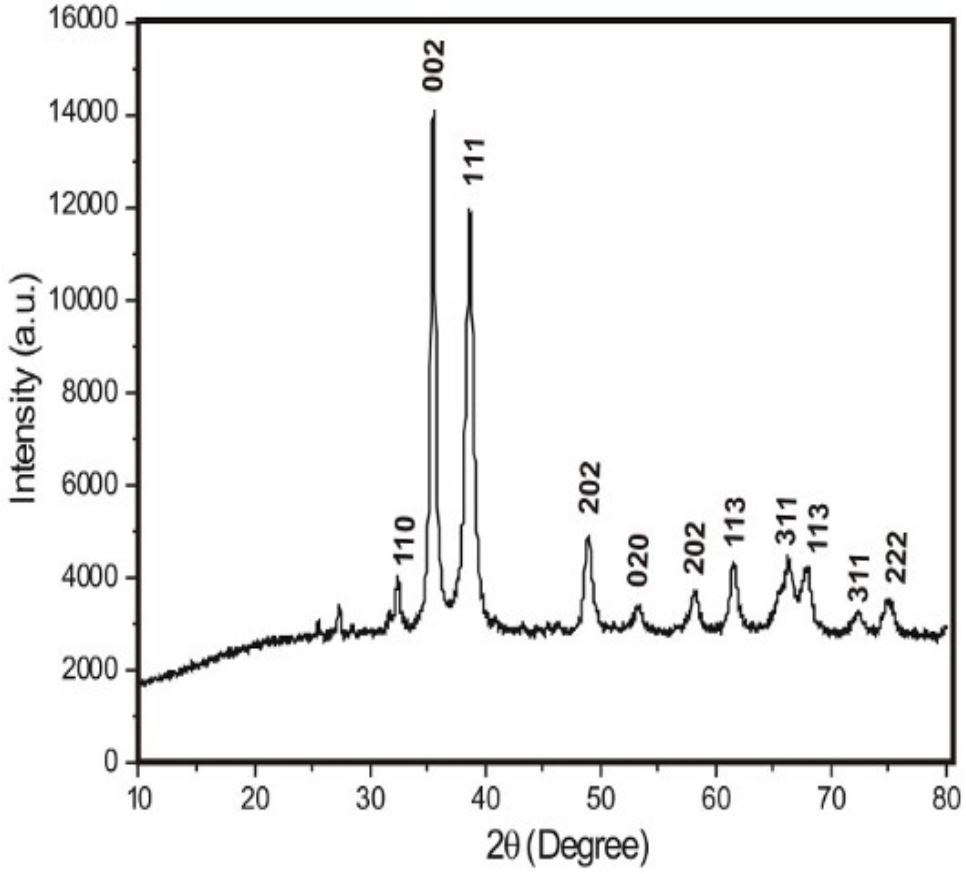

Figure 2.4: Illustration of XRD pattern using CuO nanoparticles obtained from *Calotropis gigantea* plant leaf. Reproduced with permission (Sharma et al., 2015).

different materials especially minerals and alloys. More information that can be obtained include; lattice parameters of the crystal (that determines strain and composition), misorientation (in this, studying defect types and their densities is possible) micro strain and dislocation density, wafer bowing and residual stress (Moram and Vickers, 2009).

The diffraction peak intensity is determined by how atoms are arranged in the entire crystal. A dislocation is an imperfection or defect in the crystal structure. Numerous properties of materials are significantly influenced by dislocations.

The crystallite size (D) and dislocation density (δ) can be obtained from equations (2.6) and (2.7) respectively.

$$D = \frac{K\lambda}{\beta Cos\theta} \quad \text{..... 2.6}$$

$$\delta = \frac{1}{D^2} \quad \text{..... 2.7}$$

where D is the crystallite size, K is shape factor (0.9), λ is wavelength of X-rays whose value is 1.5418 Å for Cu K_α, θ and β are diffraction angle (in degrees) and full width at half maximum (FWHM) in radians of the different peaks respectively (Bendjedidi et al., 2015).

However, the material under study undergoes strain when deposited on the glass substrate. The micro stain (ε) can also be calculated from equation 2.8.

$$\varepsilon = \frac{\beta Cos\theta}{4} \quad \text{..... 2.8}$$

where the variables are as defined above (Nabiyouni et al., 2011).

In the crystal, arrangement of atoms is in a regular repetitive manner with spacing in angstroms. Therefore, since X-rays are electromagnetic in nature and are also in angstroms, diffraction automatically occurs when X-ray beam is applied to a crystal.

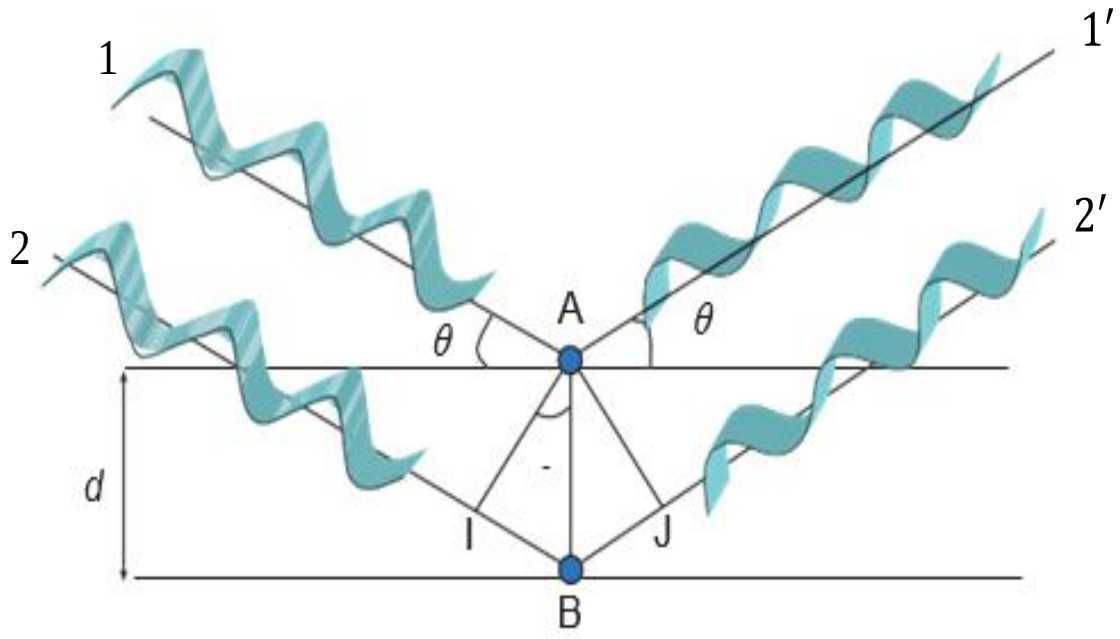

Figure 2.5: Illustration of Bragg's law. Reproduced with permission (Le Pevelen, 2010).

X-ray diffraction also occurs due to constructive interference between electromagnetic X-ray waves and the atoms of the material being studied (Bunaciu et al., 2015), and this is in line with the Bragg's law. This law is given by equation (2.9);

$n\lambda = 2d \sin\theta$ …… 2.9

where n is an integer, that is, n = 1,2,3…, λ and θ are as defined in equation (2.6) and d is the inter-atomic spacing between the crystal planes.

From Figure 2.5, constructive interference will be observed if the extra distance moved by the second ray from IB plus BJ is in integral multiples of the wavelength, λ

2.6.2 Scanning electron microscopy (SEM) and Transmission electron microscopy (TEM)

SEM (Figure 2.6) and TEM are among the most adaptable characterization techniques for materials that enable the determination and analysis the surface morphology and microstructural properties of a material (Zhou et al., 2006).

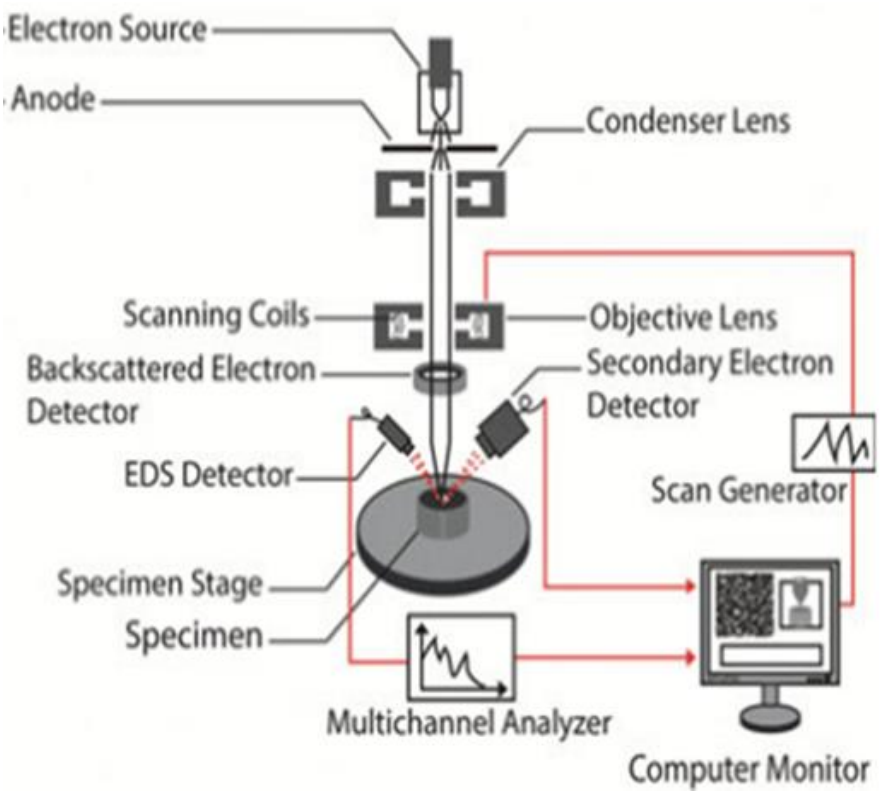

Figure 2.6: Schematic illustration of SEM. Reproduced with permission(Singh et al., 2016).

The scanning electron microscope obtains its name from scanning an energetic electron beam on a sample surface to produce images (Ul-Hamid, 2018). In fact, SEM is one of the highly preferred and reliable tools used for high-resolution imaging (resolution down to 1 nm). The disadvantage of SEM is that 1 nm resolution is at times impossible especially if samples being characterized are ordinary. This is because of the restrictions associated with the interactions between the beam and the sample which is as a result of using secondary electron signals.

To overcome this challenge, STEM-in-SEM is one approach to overcoming these constraints and enabling high-resolution imaging (Bogner et al., 2007).

Characterization using the SEM is done by focusing a beam of electrons other than the light used by optical light microscopes to give a magnified image. The image produced by the SEM depends on the signal produced by the electron and the sample being studied. The interaction is in two categories and these include elastic and inelastic interactions (scattering).

Elastic scattering is mainly due to deflection of a beam of incident electrons by sample atomic nucleus or by electrons of the outer shell of same energy while inelastic scattering is due to numerous interactions between the beam of electrons that is incident to the sample and atoms, which makes the primary beam of electron giving out a considerable quantity of energy to that atom (Zhou et al., 2006). Therefore, the main distinction between a SEM and a TEM is that while TEM uses transmitted electrons to produce images, SEM detects reflected or knocked-off electrons (electrons flowing through the sample) and TEM gives images with higher resolution (Rostamabadi et al., 2020).

2.6.3 Energy dispersive X-ray spectroscopy (EDS)

EDS, which is sometimes written as EDX or EDXS is a common technique that is commonly applied for determination and measurement of elemental composition in a sample (Figure 2.7). Elemental composition of even a very small sample of a substance including those in a cubic micrometers can be obtained (Ebnesajjad, 2011).

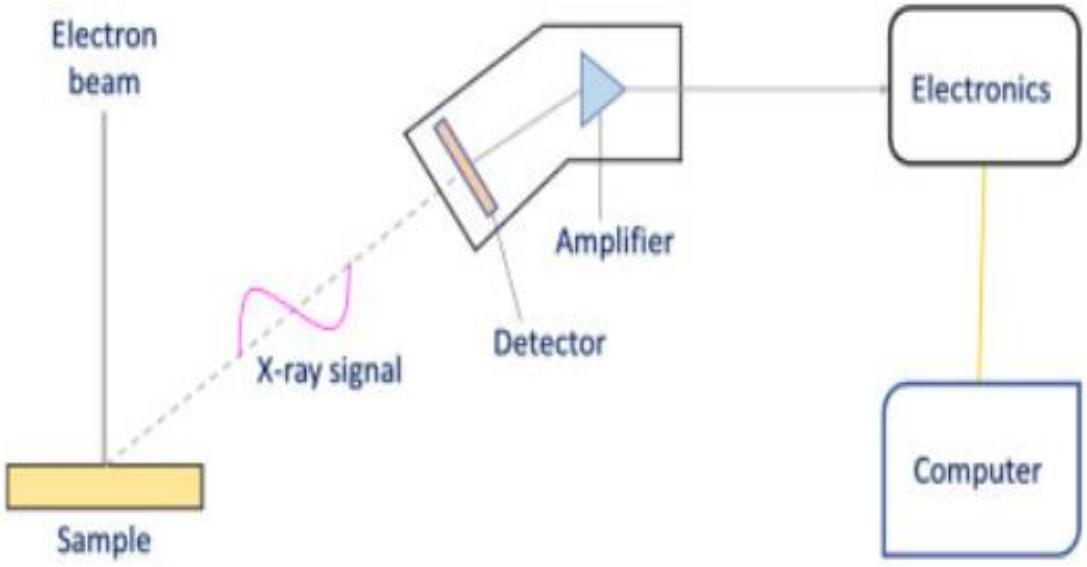

Figure 2.7: Diagrams of an EDS with the internal process involved. Reproduced with permission (Kumar et al., 2023).

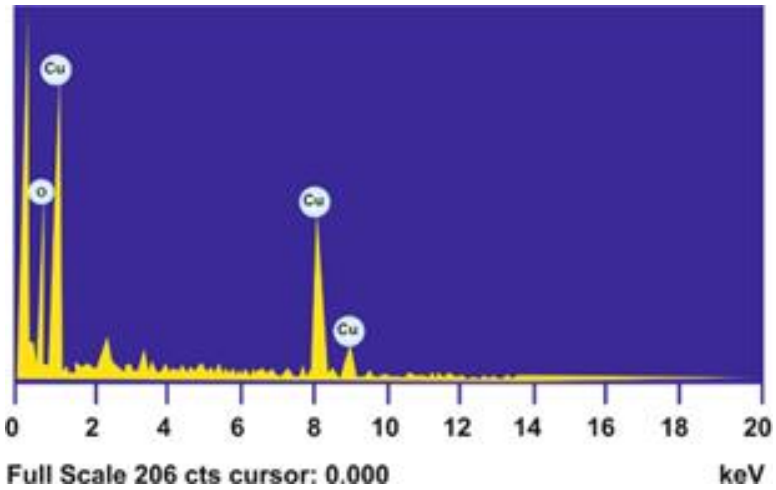

Figure 2.8: EDS spectrum for synthesized copper oxide nanoparticles. Reproduced with permission (Sagadevan et al., 2017).

EDS enables one to verify the existence of the elements in the prepared sample and to know the percentage of each element that exists in the sample. Usually, EDS systems are attached to an electron microscope, like the TEM and SEM and this depends on the emission of the specimen characteristic X-rays.

When the surface is exposed to a focused X-ray beam or a high intensity stream of charged particles, X-ray emission is stimulated. It is possible to stimulate the electrical structure of the atom to produce X-ray emissions, each having its own energy signature(Mehrban and Bowen, 2017). Figure 2.8 an example of an EDS spectrum for CuO nanoparticles.

2.6.4 UV-Visible spectroscopy

UV-Visible spectroscopy is a technique that measures how much of discrete wavelength of visible light that a sample absorbs or transmits in comparison to a reference (blank) sample. This is carried out by the using UV-Visible spectrophotometer. The transmission data can be used in calculating the absorbance (% A) of a given films for various wavelengths by using equation 2.11 (Roy et al., 2006).

$$A = 2 - log_{10}^{T} \quad \ldots\ldots 2.11$$

Also, reflectance expressed as a percentage (% R) is obtained using equation (2.12) (Abduljabbar, 2014).

$$T + A + R = 100\% \quad \text{2.12}$$

where, A and T are as defined in equation 2.11.

UV-Vis gives the optical properties of a sample and the spectral data generated can be used in determination of bandgap of a material. Other parameter that can be determined include: skin depth, extinction coefficient, dielectric constants and refractive index. Figure 2.9 shows the schematic mode of operation of a spectrophotometer.

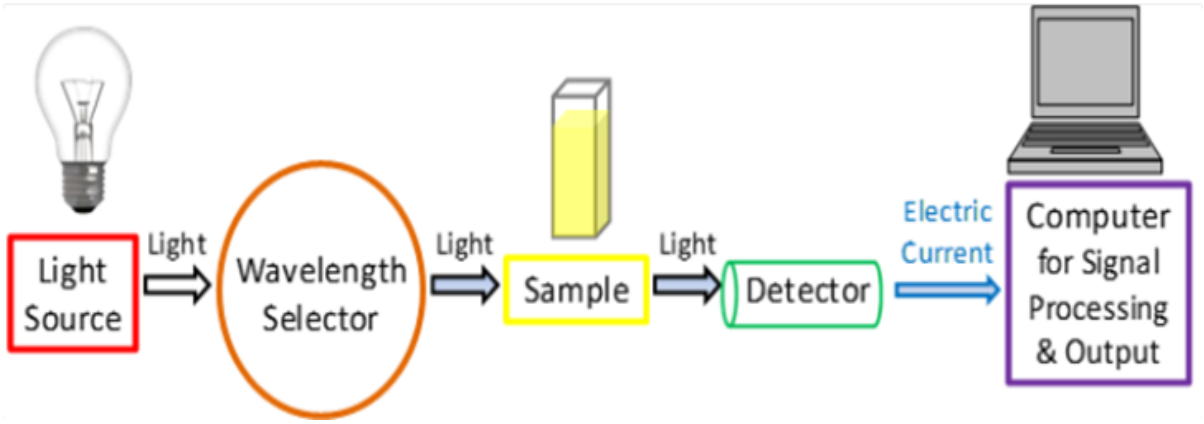

Figure 2.9: Basic elements and the light path of a visible spectrophotometer. Reproduced with permission (Grasse et al., 2016).

2.6.5 Fourier Transform Infra-red (FTIR) Spectroscopy

FTIR spectroscopy is an effective tool in material characterization applied for identification of functional groups or chemical bonds and quantification. This technique includes both absorption and reflectance spectroscopy that take place in the infrared (IR) region of the spectrum.

A sample profile or specific molecular fingerprint is created by the spectra and can be used to screen and scan samples for a number of constituents. A vibrational transition or stimulation

of a molecule to vibrational state of higher level occurs in the electromagnetic region (Shojaei and Azhari, 2018). FTIR analysis is applied in identifying several compounds in materials that could be organic, inorganic or polymeric. This is done with the help of light in the infra-red region for scanning samples. Variations in regular pattern of absorption bands evidently demonstrate a variation in the structure of material. FTIR is important not only in characterization but also for identification of unknown materials, identifying contaminants in materials, checking for additives, and identification of decomposition and oxidation (Titus et al., 2019).

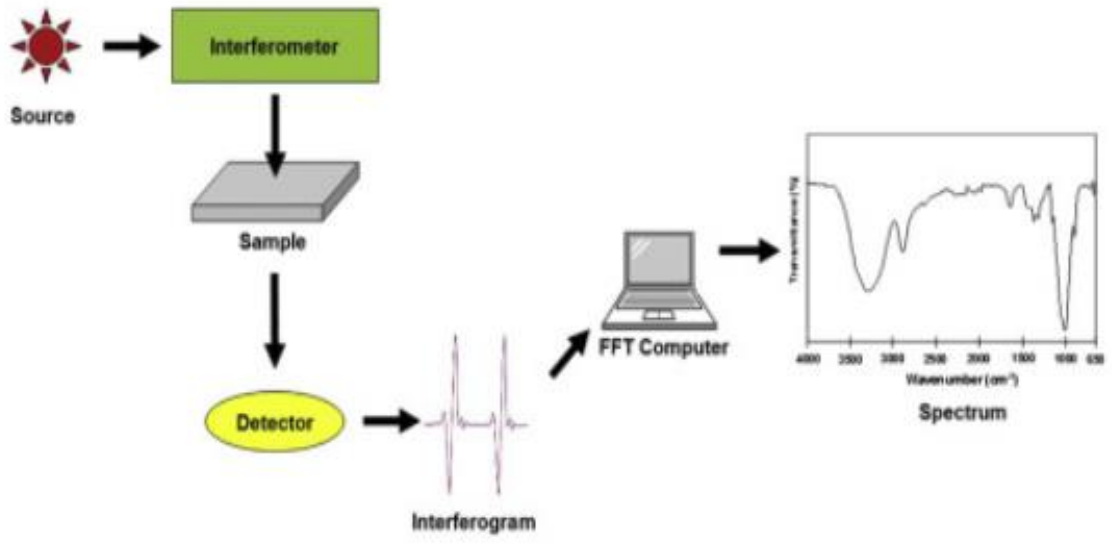

Figure 2.10: Schematic diagram of FTIR processing system. Reproduced with permission (Undavalli et al., 2021).

2.7 *I-V* Measurement

Solar Cell *I-V* measurement indicates the performance of a solar cell. It provides the relationship between the voltage applied across an electrical device and the current that flows through it. The resultant photovoltaic parameters such as J_{sc} (mA cm^2), V_{oc} (V), *FF* and *PCE* (%) can be obtained from the analysis (Sinton and Cuevas, 2000). The photocurrent–photovoltage (*J-V*) curves of DSSC or any other solar cell can be obtained by the use of the

Keithley digital source meter with illumination of a solar simulator (Song et al., 2016). Other parameters that can be obtained using the same device include; resistance, resistivity, capacitance, etc.

The above parameters can be helpful in the evaluation of the power conversion efficiency (PCE) of a solar cell using the following expression.

$$\text{Efficiency } (\eta) = \frac{P_{max}}{P_{in}} = \frac{V_{max} \times I_{max}}{Incident\ solar\ radiation \times Active\ area\ of\ the\ fabricated\ cell.}$$

$$= \frac{V_{oc} \times I_{sc} \times FF}{I_t \times A_t} \quad \ldots\ldots\ldots\ldots\ldots\ldots\ldots\ldots\ldots\ldots\ldots\ldots\ldots\ldots\ldots\ldots\ldots\ldots\ldots\ldots\ldots \; 2.13$$

where, *FF* is the fill factor and it can be obtained from, $FF = \frac{P_{max}}{V_{oc} \times I_{sc}}$

The *PCE* of the solar cell is then calculated using;

$$\text{PCE} = \frac{P_{max}}{I_t \times A_c} \quad \ldots\ldots\ldots\ldots\ldots\ldots\ldots\ldots\ldots\ldots\ldots\ldots\ldots\ldots\ldots\ldots\ldots\ldots\ldots\ldots\ldots\ldots\ldots \; 2.14$$

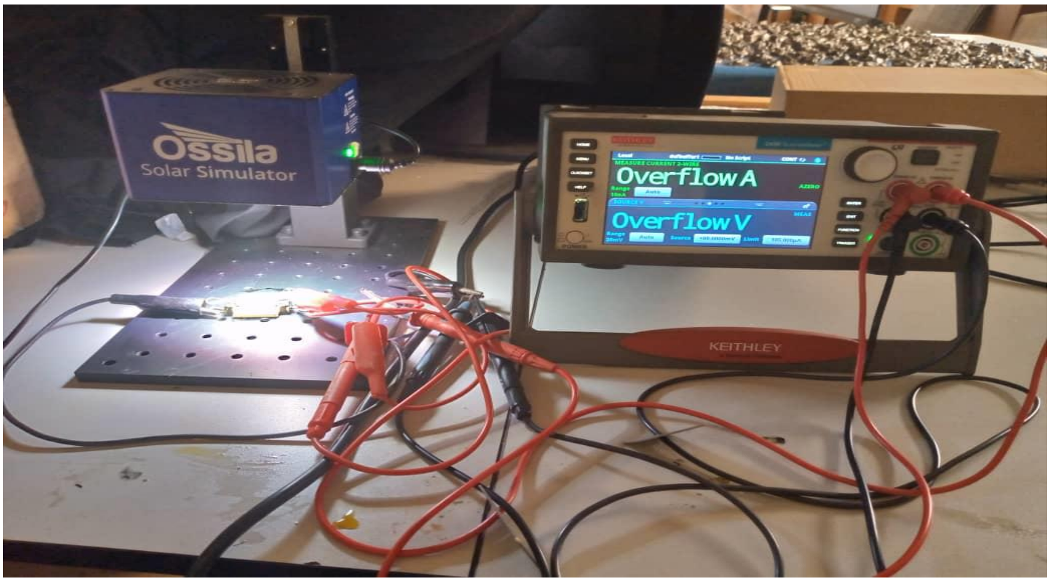

Figure 2.11: Image of a solar cell simulator and Keithley (SMU-240) for *I-V* measurement system.

From equations 2.13 and 2.14, P_{max} is the maximum power given out by the solar cell, P_{in} is power absorbed by the solar cell and V_{oc} is the output voltage (Emery and Osterwald, 1986, Devadiga et al., 2021).

Therefore, *I-V* characterization can be done using Keithley instrument which may be connected to computer under irradiation by the solar simulator or under sunshine on a clear sunny day (Figure 2.11).

CHAPTER THREE: METHODOLOGY

3.1 Introduction

This chapter presents the materials to be used, preparation of leaf extract, synthesis of CuO nanoparticles, characterization techniques that were used, fabrication of the synthesized CuO nanoparticles-based counter electrode, preparation procedures of the working electrode (photo-anode), preparation of the natural dye solution (sensitizers), preparation of liquid electrolyte, fabrication of DSSC device and measuring the current-voltage parameters.

3.2 Chemicals and materials

Cupric nitrate, ethanol (99.99% purity), polyethylene glycol (PEG), anhydrous titanium oxide powder, iodide/triiodide electrolyte, Fluorine doped tin oxide (FTO) glass substrate of sheet resistance = 6.7 ± 0.27 Ω/square cm from Ossila Ltd-UK and distilled water. TiO_2 powder < 25 nm (anatase phase). All chemicals were obtained from Sigma Aldrich and were used without further purifications. *Cucurbita maxima* plant leaves were obtained from Uganda flora and the natural dye solutions were extracted from sweet potato, pumpkin and hibiscus plant leaves (Collected from Uganda flora).

3.3 Preparation of leaf extract for synthesis of CuO nanoparticles

Freshly obtained leaves of *Cucurbita maxima* plant were washed twice using distilled water and dried under the sun so as to get rid of any remaining moisture. The dried leaves were then ground with the help of a mortar and pestle to form a powder. 500 ml of distilled water was mixed with 50 g of the powder and the mixture was heated for 60 minutes, or until the aqueous solution's colour turned from watery to yellowish. The mixture was then sieved twice using Whatman filter paper (Cat No 1001 125) to eliminate any residual solids.

3.4 Synthesis of CuO nanoparticles

50 ml of *Cucurbita maxima* leaf extract was measured and boiled between 70 and 80 ^{o}C using a hotplate fitted with a magnetic stirrer. 2.5 g of cupric nitrate were added into the solution and boiled until a yellowish-green coloured solution was obtained. The resultant solution was then placed in an oven operated at a temperature of 100 ^{o}C for 18 h until a pale green powder was obtained. The formed CuO powder was finally placed in a ceramic crucible and then annealed in a furnace at the temperature of 350 and 450 ^{o}C for 2 h.

3.5 Characterization

X-ray diffraction (XRD) was performed using an irradiation wavelength of 1.5418 Å (Cu Kα) to get data that was used to obtain the structure of the crystal, micro strain and lattice parameter of green synthesized CuO nanoparticles.

Transmission electron microscope (TEM) was also used for imaging the NPs order to obtain the particle size.

Ultra violet visible (UV-Vis) spectroscopy was carried out to find the optical properties by the use of an ultra violet UV-Visible Spectrophotometer in Diffuse Reflectance Spectroscopy (DRS) mode. The same instrument was used to determine the optical absorption properties of the natural dye solutions.

Fourier Transform Infra-red (FTIR) Spectrophotometer (IR Tracer 100) was used to determine the chemical bonds in CuO. Figure 3.1 is an image of FTIR spectrophotometer and the corresponding spectrum of CuO nanoparticles.

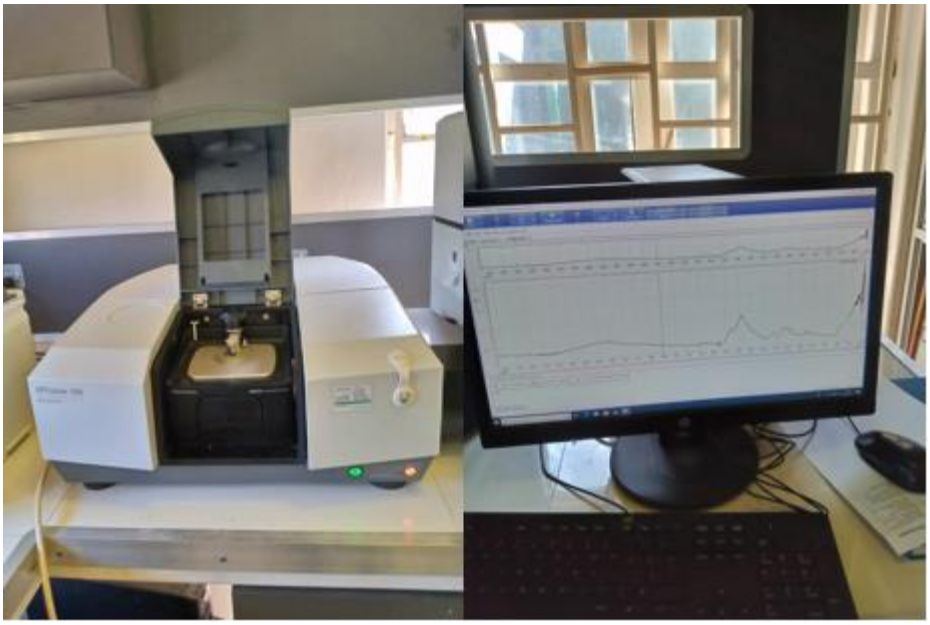

Figure 3.1: FTIR Spectrophotometer and its corresponding spectra on the screen.

3.6 Preparation of the dye solutions for use as photosensitizers

Pumpkin leaves, sweet potato leaves and hibiscus flowers were used to develop individual natural dyes solutions. Fresh pumpkin leaves, sweet potato leaves and hibiscus flowers were separately washed with distilled water and then dried inside an oven for a duration of 24 h at a temperature of 60 ^{o}C. Using a mortar and pestle, the dried leaves were ground into a fine powder. 10 g of pumpkin powder and 10 g of sweet potato leaves powder were separately dispersed in ethanol (50 ml) in an amber bottle each giving 0.2 g/ml concentration. Also, powder from hibiscus was dispersed in ethanol (100 ml) in an amber bottle to give a 0.2 g/ml concentration. The solutions in each of the bottles were kept at room temperature for 24 h in a dark place. Because of the complex nature of dye solution extraction from hibiscus, the solution was warmed at 60 ^{o}C in an incubator which was set at 150 rpm for 10 minutes and further then stored for a period of one week. All the solutions were filtered using Whatman filter paper (Cat No 1001 125) at room temperature. To avoid degradation by sun light, the solutions were separately placed in amber bottles in a dark place and kept for further use.

3.6.1 Development of composites for the dye solutions

The individual dye solutions denoted by P, S and H as the dyes extracted from pumpkin leaves, sweet potato leaves and Hibiscus flowers leaves (*Malva viscus* species) respectively were used to make composites in the mass ratios P:H-1:3 and S:H-1:3. The optical absorption properties of all the dye solutions for use as sensitizers have been discussed in chapter 4.6.

3.7 Fabrication procures for the electrode

3.7.1 Substrate cleaning

The FTO glass substrates (2.5 cm×2.5 cm^2) were rinsed with distilled water followed with ethanol for 30 minutes in an ultrasonic bath. They were then dried in an oven at 60 ^{o} C for 15 minutes. The edges of the substrates were covered with a scotch tape of thickness 0.06 mm.

3.7.2 Fabrication of counter electrode based on CuO nanoparticles

0.2 g of CuO nanoparticles were dissolved in 0.4 g of polyethylene glycol (PEG) consisting of a mixture glacial acetic acid and distilled water (5 ml for each). The resultant mixture was sonicated for 2 h and then spin coated five times each at 2,500 rpm for 10 minutes on a cleaned FTO substrate at room temperature (28 ^{o}C). The film on the substrate was annealed muffle furnace (KJ-1700) at 300 ^{o}C for 1 h. The furnace was left to cool naturally to room temperature, the film was removed and then dipped in a natural dye for 24 h. After dye absorption, the film was removed and washed in ethanol to remove residues.

3.7.3 Preparation of the working electrode

FTO glass substrate was cleaned using distilled water followed by ethanol. 1 g of TiO_2 nano-powder was dissolved in 0.4 g of polyethylene glycol consisting a mixture of 5 ml glacial acetic acid and distilled water in similar quantities. The resultant mixture was sonicated for 2 h and spin coated five times each at 2,500 rpm for 10 minutes on FTO substrate at room temperature.

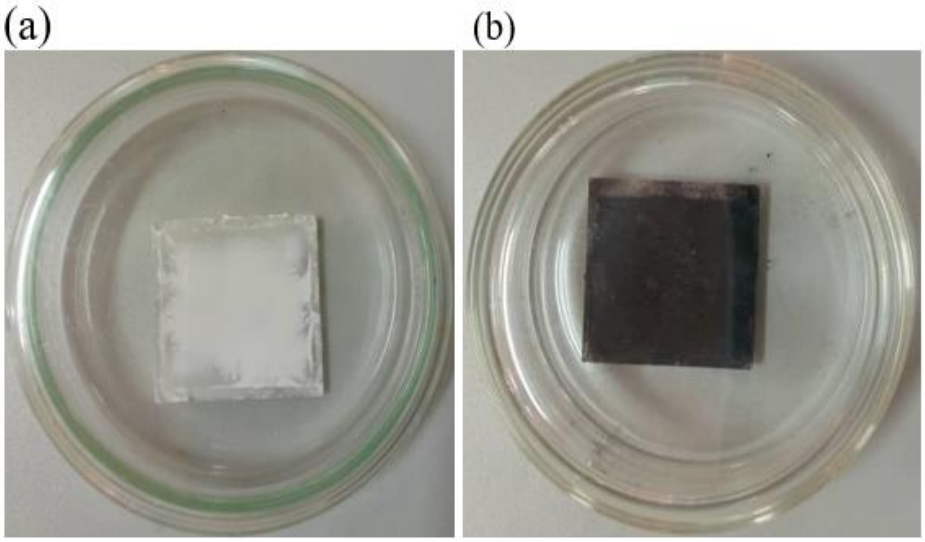

Figure 3.2: Fabricated (a) photoanode and (b) counter electrode for DSSC application.

The film on the substrate was annealed in a muffle furnace at 300 ^{o}C for 1 h. The furnace was left to cool naturally at room temperature. The annealed substrate (containing the film) was removed and kept. Figure 3.2 shows the fabricated photoanode and the counter electrode.

3.8 Preparation of liquid electrolyte

Iodine (I_2) and potassium iodide in quantities of 0.127 g and 0.83 g respectively were dissolved in ethylene glycol (10 ml) and placed in a cleaned beaker. Using a glass rod, the mixture was stirred for duration 30 minutes and then stored in a sealed bottle.

3.9 DSSC fabrication

To complete the DSSC structure, Iodine/tri-Iodine was used as the electrolyte. TiO_2, a working electrode, was sandwiched with the CuO based CE. To complete the cell fabrication, the electrolyte was applied by capillarity attraction into the space between the two prepared electrodes. I-V measurements under 1 sun illumination were recorded by Keithley digital source meter (SMU-2450). Figure 3.3 shows the whole process of synthesizing CuO nanoparticles from *Cucurbita maxima* dye extract to the final stage of device application.

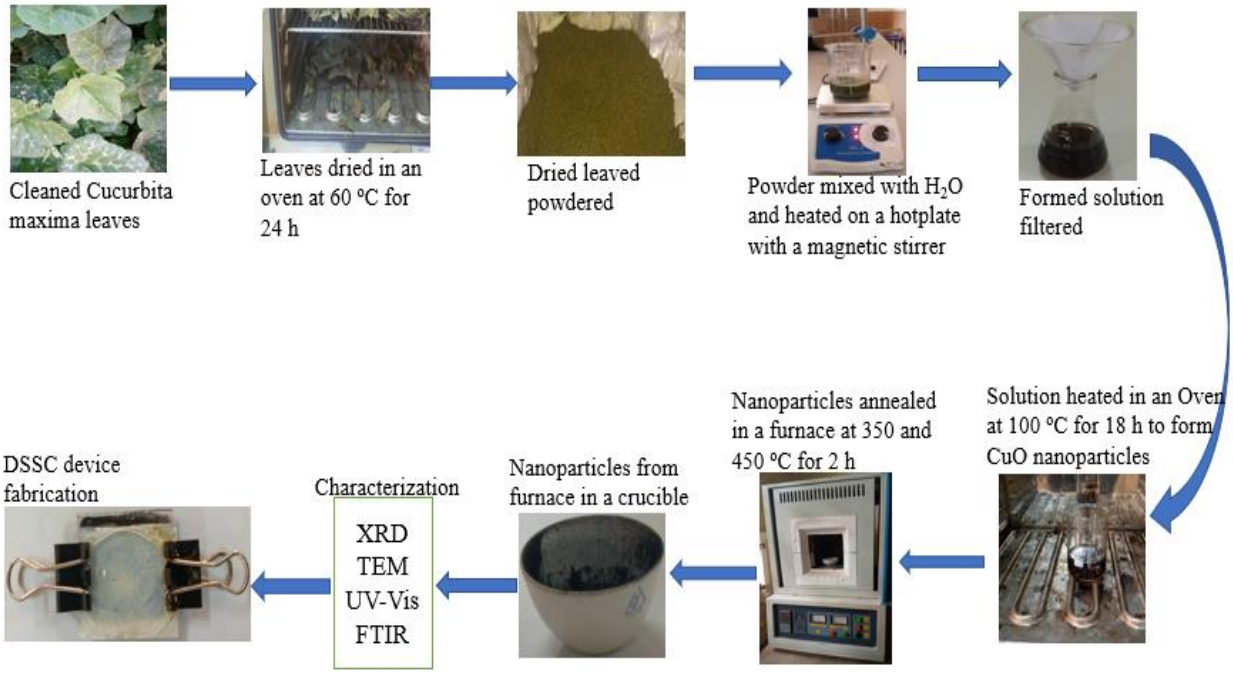

Figure 3.3: Summary of extraction process of dye solution from *Cucurbita maxima* leaves and synthesis procedure of CuO nanoparticles by green method.

CHAPTER FOUR: RESULTS AND DISCUSSION

4.1 Introduction

This chapter consists of the results and discussion on the relevant characterization techniques used in this research which include; XRD, TEM, UV-Vis Spectroscopy and FTIR. It also covers the results and analysis of DSSCs performance based on CuO CE (using different natural sensitizer) by determining their current-voltage parameters and finally determining their efficiency values.

4.2 XRD Results

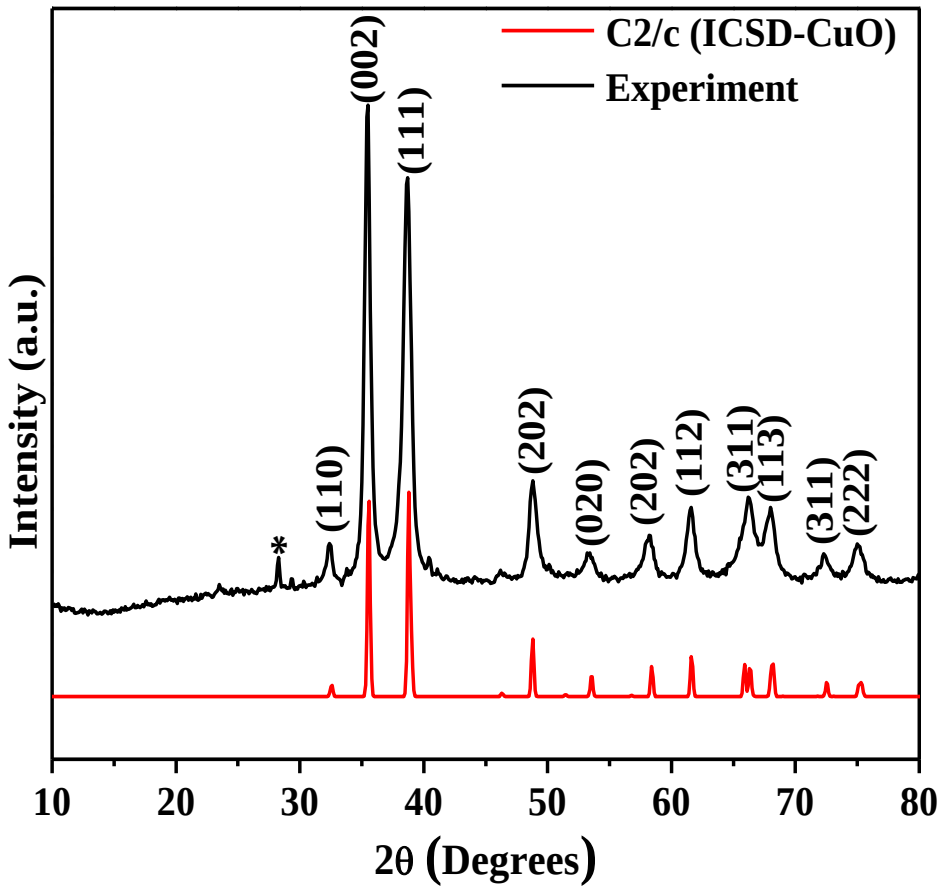

Figure 4.1: XRD pattern of CuO NPs synthesized from extract of *Cucurbita maxima* plant leaves.

The crystal structure of CuO NPs were confirmed by the characteristic peaks shown in the XRD pattern of Figure 4.1. The observed pattern in the experiment matches well with the standard pattern, ICSD No. 16025 with space group C2/c. The pattern shows various diffraction

peaks at 2θ values of 32.4º, 35.5º , 38.7º , 48.8º ,53.4º , 58.3º , 61.6º, 66.2º ,68.0º , 72.4º and 75.0º that correspond to (110), (002), (111), (202), (020), (202), (113), (311), (113), (311) and (222) planes (Sharma et al., 2015, Jeronsia et al., 2019). The extra peaks at 2θ value of 28.3 º is attributed to the impurity phase of $Cu(OH)_2$ in CuO. (Zhu et al., 2003). Additionally, the intensity of the diffraction peaks shows good crystallinity of CuO NPs. XRD data was used to obtain the average crystallite size (D), dislocation density (δ) and micro strain (ε) of the synthesized nanoparticle. The average particle size of the CuO nanoparticles was estimated according to the Debye-Scherer formula shown in equation 2.6. The dislocation density and micro strain in the film were obtained using equations 2.7 and 2.8 respectively.

Table 4.1: Results for XRD analysis of CuO nanoparticles

Peak No	Braggs Angle (2θ) (degrees)	Miller Indices (hkl)	FWHM β (2θ)	Crystallite Size (Å)	Micro Strain (%)	Dislocation Density (line/m^2)
1	32.4	110	0.564	147	0.236	4.63×10^{-5}
2	35.5	002	0.607	138	0.252	5.29×10^{-5}
3	38.7	111	0.841	100	0.346	9.95×10^{-5}
4	48.8	202	0.716	122	0.284	6.71×10^{-5}
5	53.4	020	1.115	80	0.432	1.55×10^{-4}
6	58.3	202	0.733	124	0.279	6.48×10^{-5}
7	61.6	113	0.727	127	0.272	6.16×10^{-5}
8	66.2	311	1.363	70	0.498	2.06×10^{-4}
9	68.0	113	0.952	101	0.344	9.85×10^{-5}
10	72.4	311	0.901	109	0.317	8.37×10^{-5}
11	75.0	222	1.086	92	0.375	1.17×10^{-4}

The obtained values of the crystallite size, micro strain, and dislocation density are 10.8 ± 0.1 nm, 0.367%, and 1.26×10^{-4} line/m^2 respectively. The crystallite size value obtained agrees well to the TEM value for both samples annealed at 450 ^{o} C (9.1nm).

4.3 TEM Results

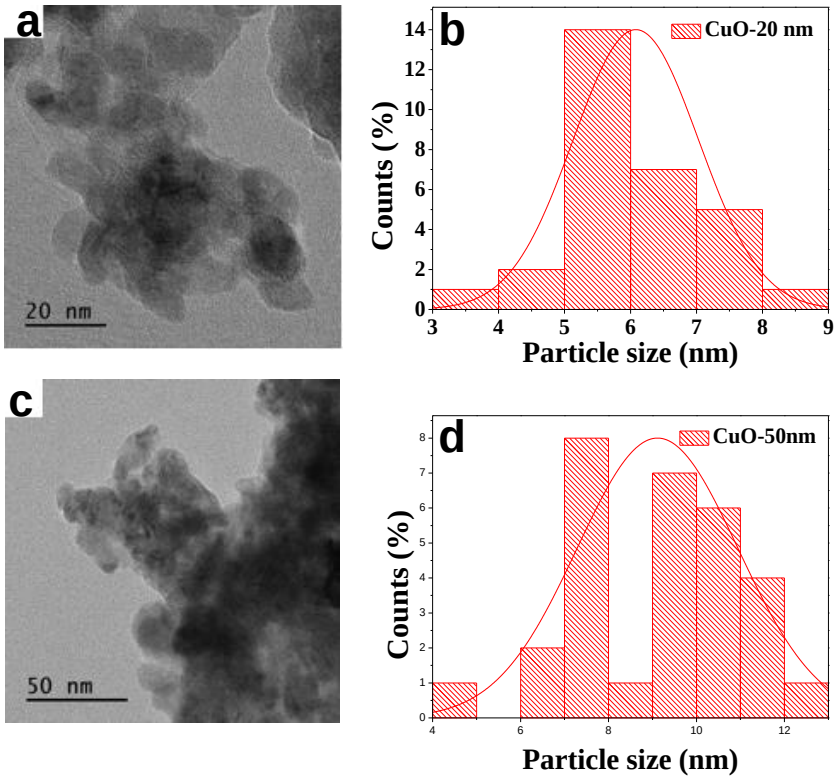

Figure 4. 2: (a) TEM image for CuO nanoparticles annealed at 350 ℃, (c) TEM image for CuO nanoparticles annealed at 450 ℃, (b) Histogram for particle size distribution for sample annealed at 350 ℃ and (d) Histogram for particle distribution for sample annealed at 450 ℃.

TEM studies were carried out to examine the morphology and size of the synthesized CuO nanoparticles as seen in Figure 4.2. The TEM images reveal CuO NPs with spherically shaped and agglomerated particles. The average particle size at annealing temperature of 350 and 450 ℃ were 6.1 ± 0.1 and 9.1 ± 0.1 nm respectively.

The increase in particle size is thermodynamically caused by increase in temperature. In general, the size of CuO NPs achieved using *Cucurbita maxima* plant extract is smaller compared to previous reports (Das et al., 2013, Sharma et al., 2015, Andualem, 2020).

4.4 Optical properties

Figure 4.3 (a) shows the diffuse reflection spectra (DRS) of CuO nanoparticles for the as synthesized sample (at room temperature before annealing), annealed at 350 and 450 ℃. A sharp peak is observed at 536 nm for the as synthesized sample. The peak disappears with the increase in annealing temperature. The disappearance of the peak is due phase formation at 350 ℃, which stabilizes at 450 ℃. The sharp peak at RT is a related to surface Plasmon resonance absorption of metal oxide nanoparticles, normally observed when the wavelength of the is greater than the particle size on the material (Das et al., 2013, Hou and Cronin, 2013). An absorption spectrum is shown in Figure 4.3 (b) was obtained using the Kubelka-Munk (KM) function (Džimbeg-Malčić et al., 2011). The KM function is given by equation (4.1).

$$F(R) = \frac{K}{S} = \frac{(1-R)^2}{2R} \quad \text{4.1}$$

where F(R) is the Kubelka Munk function which is the ratio of absorption coefficient K, to scattering coefficient S and R is reflectance.

The band gap was computed by making a Tauc plot given by equation (4.2).

$$(F(R)hv)^r = A(hv) \quad \text{4.2}$$

where hv is the optical energy, A is a constant and r is equal to 2 if the transition is a direct one or 1/2 if the transition is indirect.

The energy bandgap energy (E_g) of CuO nanoparticles was obtained by extrapolating the linear parts of the graphs obtained from Equation (4.2). Figure 4.3 (c) shows the Tauc plot for CuO nanoparticles at annealing temperatures of 350 and 450 ℃. A band gap of 1.56 eV was estimated from Tauc plot for both samples.

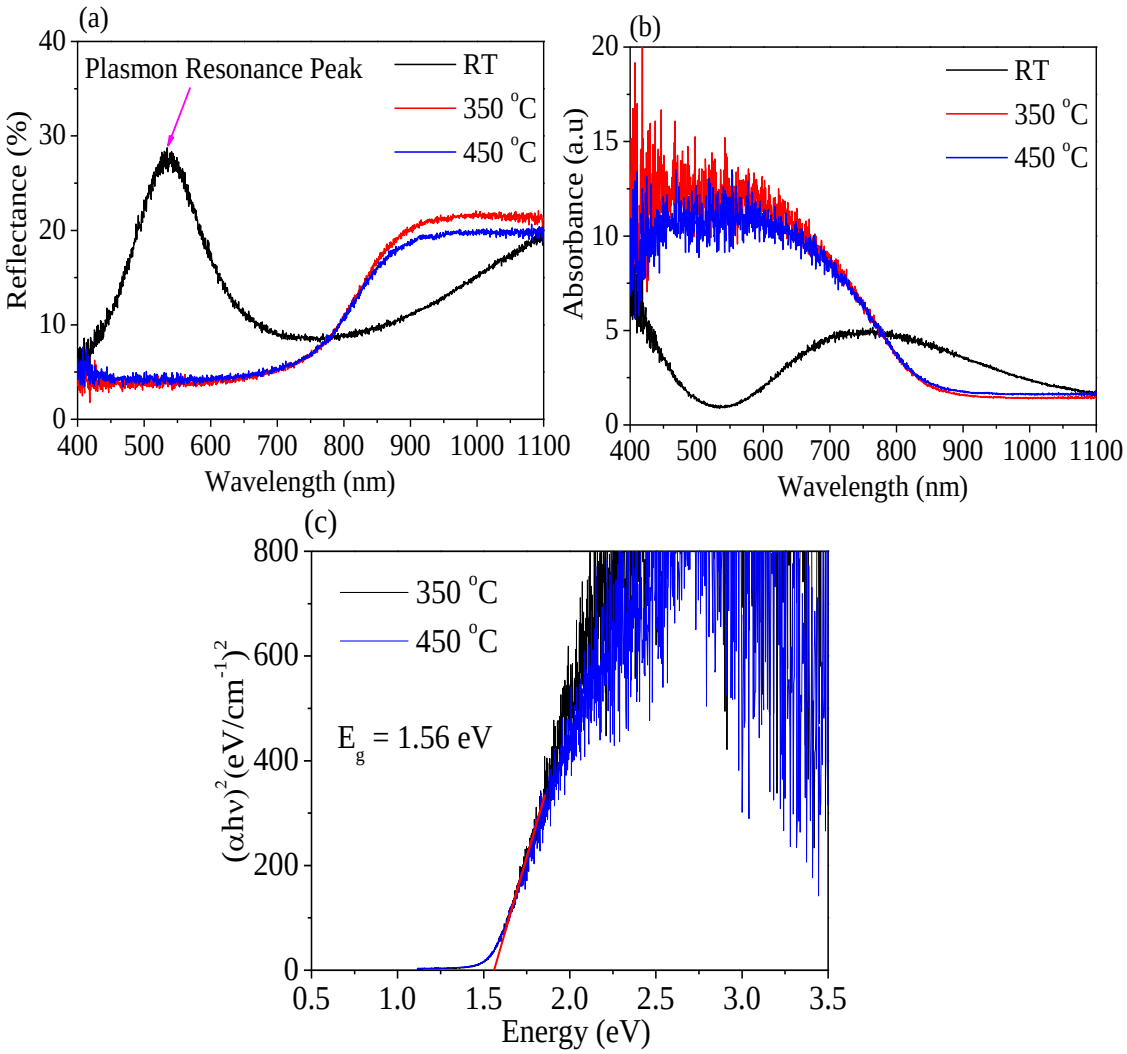

Figure 4.3: (a) Reflectance versus wavelength of CuO NPs at different temperatures, (b) Absorbance versus wavelength for CuO NPs at different temperatures and (c) Tauc plot for CuO NPs at 350 and 450 ℃.

The values of the bandgap energy (E_g) obtained are all higher than the bulk CuO with E_g=1.2 eV (Mohamed et al., 2021). The increase is attributed to quantum size effects in nanomaterials (Mukhokosi et al., 2017, Maaza et al., 2022).

4.5 Fourier Transform Infrared (FTIR) results

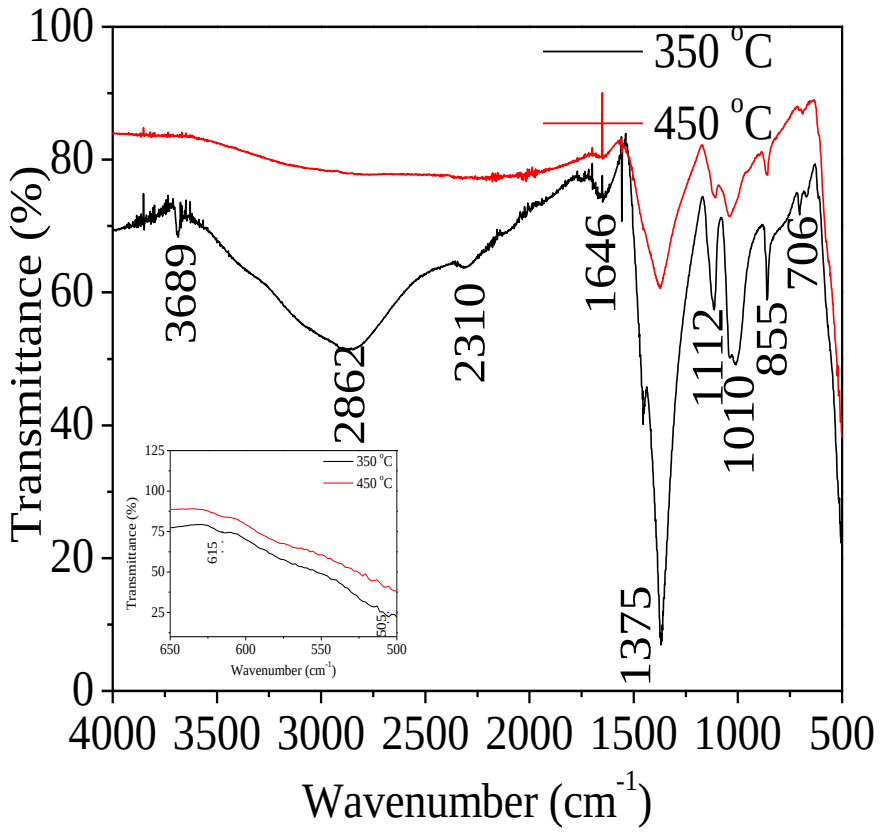

Figure 4. 4: FTIR spectra for CuO nanoparticles annealed at 350 and 450 ℃

Figure 4.6 shows the Fourier Transform Infra-red (FTIR) Spectroscopy CuO NPs at two different synthesis temperatures. A sharp peak at 3689 cm^{-1} is assigned to the asymmetric stretching of the O-H bond in alcohols (Andualem, 2020, Hou and Cronin, 2013). The broad peak at 2856 cm^{-1} is due to the C–H stretching bond. The peak at 2350 cm^{-1} is due to C=O stretch and indicates the presence of alkanes while the peaks at 1646 cm^{-1} is assigned to C-C bond and shows the presence of alkenes (Kumar et al., 2015). The peak at 1357 cm^{-1} is assigned to C-N bond and indicates the presence of amine groups (Andualem, 2020). Peaks located at 1112 $cm^{-1}$is due to Cu–OH bond (Gowri et al., 2019) and the peak at 1010 cm^{-1} is assigned to CuO bond (Hou and Cronin, 2013). A vibration band at 855 cm^{-1} is assigned to –CH bending vibration (Gowri et al., 2019). A vibration band at 706 cm^{-1} is attributed to alcohol and phenolic groups, C–N stretching in amines (Vishveshvar et al., 2018).

4.6 Optical absorption properties of dyes extracted from pumpkin leaves, sweet potato leaves, hibiscus flowers and their composites

4.6.1 Optical absorption properties of individual dye extracts

Figure 4.7 shows the characteristics of absorbance of pumpkin, sweet potato and hibiscus dye. Figure 4.7 (a) shows the spectrum for pumpkin, having two maximum absorption peaks at 469 and 661 nm. The maximum absorption peaks for sweet potato spectrum also correspond to two wavelength values, at 421 and 665 nm (Figure 4.7 (b)). This implies that in both spectra (pumpkin and sweet potato), colours in the blue and red region of the visible spectrum are absorbed and green colour is reflected which is a characteristic of chlorophyll pigment. The maximum absorption peaks for both spectra obtained correlate well with earlier reported results (Clementson and Wojtasiewicz, 2019, Palupi et al., 2020, Lai et al., 2008). From Figure 4.7 (c), the maximum absorption peak for hibiscus is observed at 525 nm. This shows that green and adjacent colours are absorbed and red in hibiscus is reflected which implies the presence of anthocyanin pigment in hibiscus.

The absorption peak obtained corresponds well with first reports (Yuniati et al., 2021, Munandar et al., 2022). It is noted that the optical characterization of all the three dyes revealed

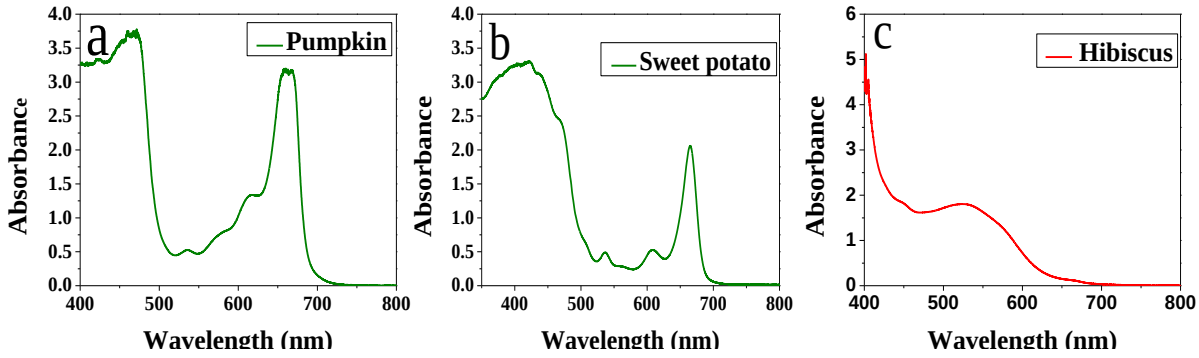

Figure 4.5: Absorption spectrum for dye extracts of (a) pumpkin dye extract, (b) sweet potato and (c) hibiscus flowers.

high absorbance within the visible (VIS) region of the spectrum, hence making them suitable candidates for photovoltaic solar cell devices.

4.6.2 Optical absorption properties of dye extract composite

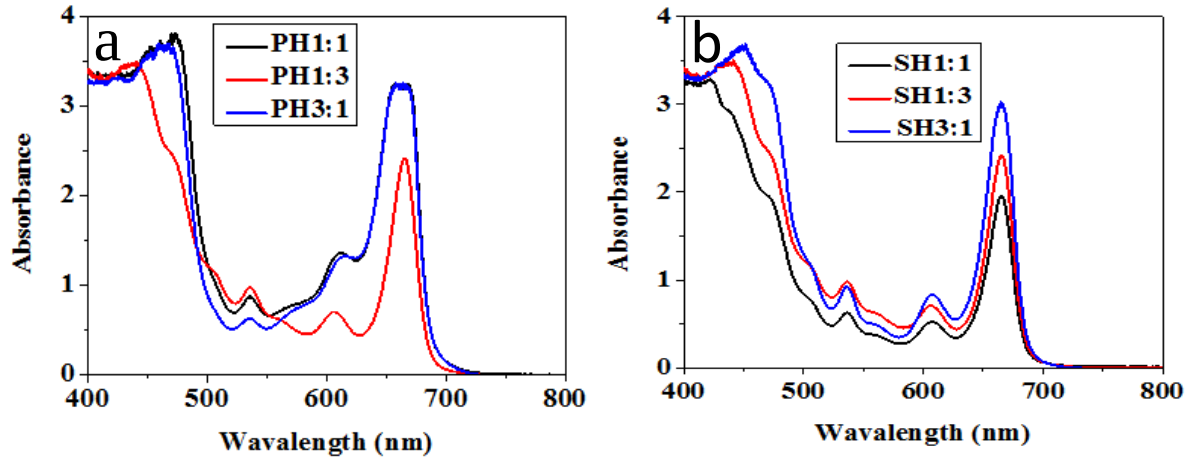

Figure 4. 6: Absorption spectra for (a) pumpkin and hibiscus composite, (b) sweet potato and hibiscus composite at various ratios.

In Figure 4.8 (a) different ratios of 1:1, 1:3 and 3:1 were used for this mixture by optimization. It was observed that mixture of chlorophyll and anthocyanin dyes leads to absorption of photons in the green region which were previously reflected by the single chlorophyll dye and also extends the absorption range of hibiscus. As a result, a red shift from about 661 nm to between 663-665 nm giving a difference of 2-4 nm. The red shift is due to presence of anthocyanin and chlorophyll interaction while the slightly increased wavelength allows wide range of absorption of energy of the sun which could have led to improved efficiency of a solar cell.

For composite in Figure 4.8 (b), there is a red shift from 665 nm to 666 nm, giving a difference of 1 nm. The red shift is due to presence of anthocyanin and chlorophyll interaction. The slightly increased wavelength allows wide range of absorption of the energy from the sun which could lead to improved efficiency of a solar cell.

4.7 Power conversion efficiency (PCE) of DSSCs developed from CuO nanoparticles using natural dyes as the sensitizer

Figure 4.9 (a and b) show the *J-V* and *P-V* characteristics of the fabricated solar cell using CuO as the counter electrode. The PCE of the fabricated DSSCs were obtained using the expression in equation 2.13. The active area of the devices was 4 cm $^{-2}$. The open circuit voltage and short circuit current density were determined using the *J-V* characteristic graph as observed in Figure 4.9 (a and b) respectively. The open circuit voltage and short circuit current density were determined

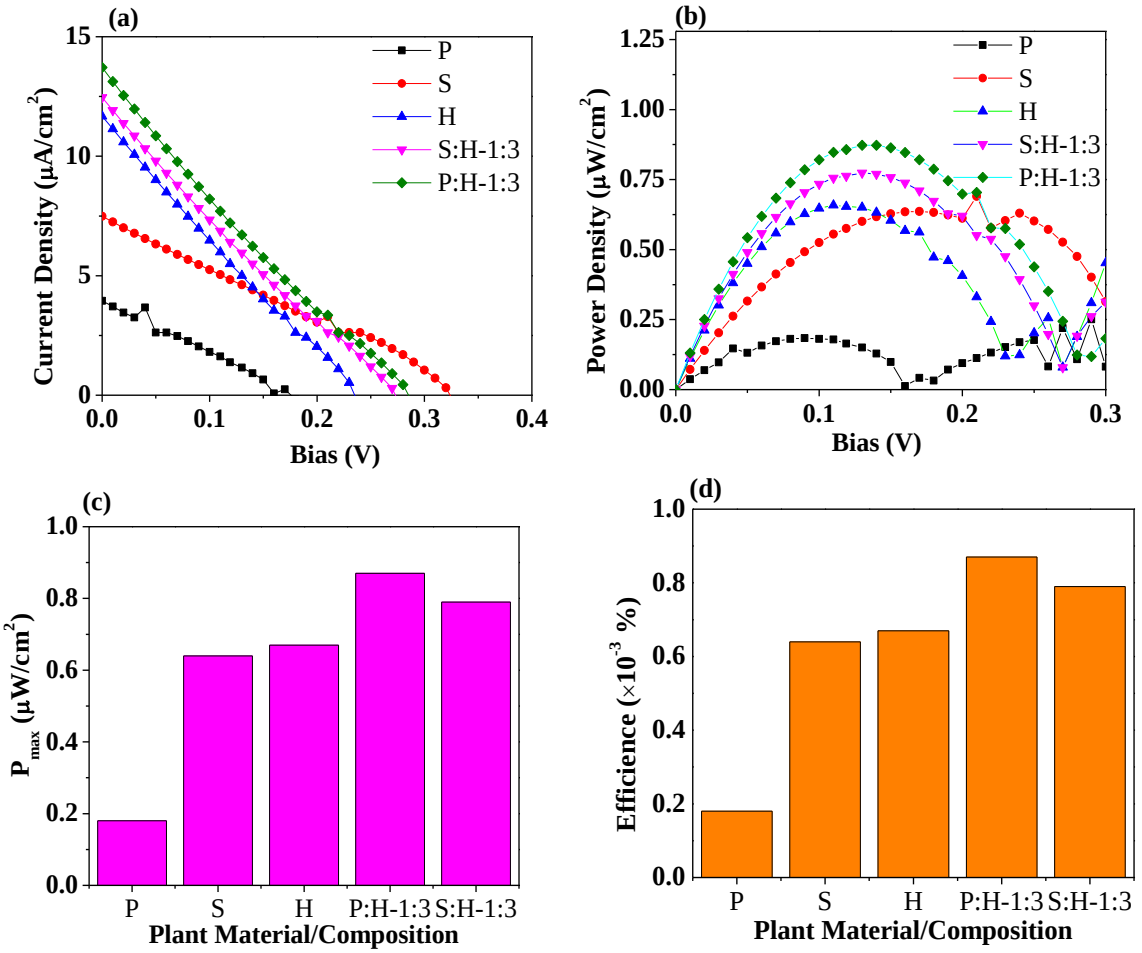

Figure 4.7: (a) *J-V* characteristic curve. (b) *P-V* characteristic curve. (c) Bar graph of maximum power and (d) Bar graph of power conversion efficiency of plant materials.

from the *J-V* characteristic graph as shown in Figure 4.9 (a). The DSSC devices based on CuO CE fabricated using individual dyes as sensitizer, Hibiscus (H) based DSSC had a maximum PCE of 6.7×10^{-4} %. This was followed by sweet potato (S) with a PCE of 6.4×10^{-4} % and lastly pumpkin (P) with a PCE of 1.8×10^{-4} %.

With all the individual dyes, highest PCE in hibiscus (H) based DSSC is attributed to a wide range of photons that are absorbed within the visible region of the electromagnetic spectrum and the effective binding of the dye with the photoelectrode resulting into a higher short circuit current density as evidenced in Figure 4.9 (a) and better device performance. Figure 4.9 (d) shows that the CuO CE based DSSCs fabricated from dye composites have better PCE than the individual dyes. The cell device using P:H-1:3 dye composite attained the best PCE of 8.7×10^{-4} % compared to the 7.9×10^{-4} % of S:H composite based DSSC. The effectiveness in performance of composite-based DSSCs is attributed to a combination of anthocyanin and chlorophyll dyes, which exhibit an increase in the absorption wavelength range compared to the absorption wavelength range of the individual dyes. As a result, a higher short circuit current density (J_{sc}) and better PCE were attained. However, the general trend for DSSCs fabricated using natural dyes have low efficiency values since the transfer of electrons by the natural dye in the TiO_2 semiconductor layer is not so effective as compared to the standard ruthenium dye (Trihutomo et al., 2019). Table 4.3 is a summary of the results obtained during photovoltaic measurement of DSSCs fabricated in this study. The results are summarized as shown in table 4.2.

Table 4.3 shows the comparison of efficiency values for some few selected DSSCs based on different natural dye (sensitizers) as photon absorbers and the results obtained in this study are comparable to what other researchers have obtained using Pt as CE

Table 4. 2: PCE performances of DSSCs based on different natural sensitizers

Dye (sensitizer)	J_{sc}(μA/cm^2)	V_{oc}(V)	P_{max}(mW/cm^2)	η (%)
Sweet potato leaves	7.6	0.33	0.64	6.4×10^{-4}
Pumpkin leaves	4.2	0.17	0.18	1.8×10^{-4}
Hibiscus flowers	11.91	0.23	0.67	6.7×10^{-4}
Sweet potato plus Hibiscus leaves	12.5	0.27	0.79	7.9×10^{-4}
Pumpkin plus Hibiscus leaves	13.94	0.29	0.87	8.7×10^{-4}

Table 4. 3: Comparison of efficiency values for some few selected DSSCs based on natural dyes.

Counter electrode	Dye	*PCE* (%)	Reference
Pt	Strobilanthes cusia	1.18×10^{-2}	(Mejica et al., 2023)
Pt	Ocimum Gratissimum	2.1×10^{-2}	(Eli et al., 2016)
Graphite	Strobilanthes cusia	3.85×10^{-2}	(Mejica et al., 2023)
Carbon	Brassica oleracea var	5.4×10^{-2}	(Pratiwi et al., 2016)
Carbon	Turmeric	2.0×10^{-3}	(Hossain et al., 2017)
Carbon soot	Mangifera indica	2.35×10^{-4}	(Morka et al., 2022)
Carbon soot	Manihot esculenta	2.35×10^{-5}	(Morka et al., 2022)
CuO	Pumpkin leaves	1.8×10^{-4}	This study
	Sweet potato leaves	6.4×10^{-4}	
	Hibiscus flowers	6.7×10^{-4}	
	Pumpkin plus Hibiscus leaves	8.7×10^{-4}	
	Sweet potato plus Hibiscus leaves	7.9×10^{-4}	

CHAPTER FIVE: CONCLUSION AND RECOMMENDATION

5.1 Introduction

With reference to the investigations carried out, the chapter addresses the conclusions and recommendations.

5.2 Conclusion

In this study, uniform distributed CuO NPs of $< 10\ nm$ were synthesized from aqueous leaf extract of Cucurbita maxima plant and applied it as a CE in DSSCs. The synthesized NPs were characterized by various tools that include XRD, TEM, UV-Visible spectrophotometer and FTIR. The XRD results revealed a monoclinic phase of space group C2/c with average particle size of 10.8 ± 0.1 nm and the average particle size from the TEM results were 6.1 ± 0.1 and 9.1± 0.1 nm at synthesis temperatures of 350 and 450 ^{o}C respectively. The optical properties revealed bandgaps of 1.56 for both the annealing. FTIR showed peaks that confirmed the bonding vibrations present in CuO NPs. The DSSC based on CuO NPs with P:H-1:3 composite dyes exhibited the highest PCE of 0.18 mW/cm^2 with an open circuit voltage of 0.17 V and a short circuit current density of 0.18 μA cm^{-2} under standard test conditions. Therefore, the results of this study show the green synthesis approach in synthesizing CuO NPs and developing a CE can be a good alternative to other synthesis procedures and an alternative to Pt for DSSC application.

5.3 Recommendation

There is need for further studies on green synthesis of CuO using other plant leaves and materials in order to find more plant materials that can give other morphologies of CuO NPs

Similar work can be done using a standard dye rather than a natural dye in order to improve the values of efficiency obtained in this research. Further studies can be carried out on synthesis of CuO from *Cucurbita maxima* dye extract with other material or compound to form a

composite of CuO with another element with good electrical properties to improve the photo-to-electric conversion efficiency in DSSCs.

Finally, its recommended that same work can be done by using other methods of thin film preparation so as to study the variation of efficiency with different thin film preparation methods.

REFERENCES

ABBOUD, Y., SAFFAJ, T., CHAGRAOUI, A., EL BOUARI, A., BROUZI, K., TANANE, O. & IHSSANE, B. 2014. Biosynthesis, characterization and antimicrobial activity of copper oxide nanoparticles (CONPs) produced using brown alga extract (Bifurcaria bifurcata). *Applied nanoscience,* 4**,** 571-576.

ABDULJABBAR, L. M. 2014. Study the effect of annealing on optical and electrical properties of ZnS thin film prepared by CO2 laser deposition technique. *Iraqi Journal of Laser,* 13**,** 29-35.

ALI, N., HUSSAIN, A., AHMED, R., WANG, M., ZHAO, C., HAQ, B. U. & FU, Y. Q. 2016. Advances in nanostructured thin film materials for solar cell applications. *Renewable and Sustainable Energy Reviews,* 59**,** 726-737.

AN, G.-H., AN, H. & AHN, H.-J. 2016. Ruthenium nanofibers as efficient counter electrodes for dye-sensitized solar cells. *Journal of Electroanalytical Chemistry,* 775**,** 280-285.

ANDUALEM, W. W. 2020. GREEN SYNTHESIS OF CUO NANOPARTICLES FOR THE APPLICATION OF DYE SENSITIZED SOLAR CELL.

BALYEJJUSA, S. M. 2015. Uganda's vision 2040 and human needs promotion. *Africa Development,* 40**,** 61-90.

BENDJEDIDI, H., ATTAF, A., SAIDI, H., AIDA, M., SEMMARI, S., BOUHDJAR, A. & BENKHETTA, Y. 2015. Properties of n-type SnO2 semiconductor prepared by spray ultrasonic technique for photovoltaic applications. *Journal of Semiconductors,* 36**,** 123002.

BOGNER, A., JOUNEAU, P.-H., THOLLET, G., BASSET, D. & GAUTHIER, C. 2007. A history of scanning electron microscopy developments: Towards "wet-STEM" imaging. *Micron,* 38**,** 390-401.

BRITTO-HURTADO, R. & CORTEZ-VALADEZ, M. 2022. Green synthesis approaches for metallic and carbon nanostructures. *Green Functionalized Nanomaterials for Environmental Applications.* Elsevier.

BUNACIU, A. A., UDRIŞTIOIU, E. G. & ABOUL-ENEIN, H. Y. 2015. X-ray diffraction: instrumentation and applications. *Critical reviews in analytical chemistry,* 45**,** 289-299.

CAI, H., LI, J., WANG, R., WU, F. & TONG, X. 2017. Copper-doped iron carbide as counter electrodes for dye-sensitized solar cells. *Int J Electrochem Sci,* 12**,** 8421-8431.

CAO, P., PENG, J., LI, J. & ZHAI, M. 2017. Highly conductive carbon black supported amorphous molybdenum disulfide for efficient hydrogen evolution reaction. *Journal of Power Sources,* 347**,** 210-219.

CHEN, J.-Z., WANG, C., HSU, C.-C. & CHENG, I.-C. 2016. Ultrafast synthesis of carbon-nanotube counter electrodes for dye-sensitized solar cells using an atmospheric-pressure plasma jet. *Carbon,* 98**,** 34-40.

CLEMENTSON, L. A. & WOJTASIEWICZ, B. 2019. Dataset on the absorption characteristics of extracted phytoplankton pigments. *Data in brief,* 24**,** 103875.

DAS, D., NATH, B. C., PHUKON, P. & DOLUI, S. K. 2013. Synthesis and evaluation of antioxidant and antibacterial behavior of CuO nanoparticles. *Colloids and Surfaces B: Biointerfaces,* 101**,** 430-433.

DEVADIGA, D., SELVAKUMAR, M., SHETTY, P. & SANTOSH, M. 2021. Dye-sensitized solar cell for indoor applications: a mini-review. *Journal of Electronic Materials,* 50**,** 3187-3206.

DŽIMBEG-MALČIĆ, V., BARBARIĆ-MIKOČEVIĆ, Ž. & ITRIĆ, K. 2011. Kubelka-Munk theory in describing optical properties of paper (I). *Tehnički vjesnik,* 18**,** 117-124.

EBNESAJJAD, S. 2011. Surface and material characterization techniques. *Handbook of Adhesives and Surface Preparation.* Elsevier.

ELI, D., MUSA, G. P. & EZRA, D. 2016. Chlorophyll and betalain as light-harvesting pigments for nanostructured TiO2 based dye-sensitized solar cells. *Journal of Energy and Natural Resources,* 5**,** 53-58.

EMERY, K. & OSTERWALD, C. 1986. Solar cell efficiency measurements. *Solar Cells,* 17**,** 253-274.

GAO, M., SUN, L., WANG, Z. & ZHAO, Y. 2013. Controlled synthesis of Ag nanoparticles with different morphologies and their antibacterial properties. *Materials Science and Engineering: C,* 33**,** 397-404.

GIELEN, D., BOSHELL, F., SAYGIN, D., BAZILIAN, M. D., WAGNER, N. & GORINI, R. 2019. The role of renewable energy in the global energy transformation. *Energy Strategy Reviews,* 24**,** 38-50.

GOWRI, M., LATHA, N. & RAJAN, M. 2019. Copper oxide nanoparticles synthesized using Eupatorium odoratum, Acanthospermum hispidum leaf extracts, and its antibacterial effects against pathogens: a comparative study. *BioNanoScience,* 9**,** 545-552.

GRASSE, E. K., TORCASIO, M. H. & SMITH, A. W. 2016. Teaching UV–Vis spectroscopy with a 3D-printable smartphone spectrophotometer. *Journal of Chemical Education,* 93**,** 146-151.

HALME, J., VAHERMAA, P., MIETTUNEN, K. & LUND, P. 2010. Device physics of dye solar cells. *Advanced materials,* 22**,** E210-E234.

HOSSAIN, M. K., PERVEZ, M. F., TAYYABA, S., UDDIN, M. J., MORTUZA, A., MIA, M., MANIR, M., KARIM, M. & KHAN, M. A. 2017. Efficiency enhancement of natural dye sensitized solar cell by optimizing electrode fabrication parameters. *Mater. Sci,* 35**,** 816-823.

HOU, W. & CRONIN, S. B. 2013. A review of surface plasmon resonance-enhanced photocatalysis. *Advanced Functional Materials,* 23**,** 1612-1619.

ITO, S., NAZEERUDDIN, M. K., LISKA, P., COMTE, P., CHARVET, R., PÉCHY, P., JIROUSEK, M., KAY, A., ZAKEERUDDIN, S. & GRÄTZEL, M. 2006. Prog. Photovoltaics. press.

JERONSIA, J. E., JOSEPH, L. A., VINOSHA, P. A., MARY, A. J. & DAS, S. J. 2019. Camellia sinensis leaf extract mediated synthesis of copper oxide nanostructures for potential biomedical applications. *Materials Today: Proceedings,* 8**,** 214-222.

KAKIAGE, K., AOYAMA, Y., YANO, T., OYA, K., FUJISAWA, J.-I. & HANAYA, M. 2015. Highly-efficient dye-sensitized solar cells with collaborative sensitization by silyl-anchor and carboxy-anchor dyes. *Chemical communications,* 51**,** 15894-15897.

KALYANASUNDARAM, K. 2010. *Dye-sensitized solar cells,* CRC press.

KAY, A. & GRÄTZEL, M. 1996. Low cost photovoltaic modules based on dye sensitized nanocrystalline titanium dioxide and carbon powder. *Solar Energy Materials and Solar Cells,* 44**,** 99-117.

KHALED, N., PATTEL, B. & SIDDIQUI, A. 2020. *Digital twin development and deployment on the cloud: developing cloud-friendly dynamic models using Simulink®/SimscapeTM and Amazon AWS,* Academic Press.

KIM, A. R., VINOTHKANNAN, M. & YOO, D. J. 2018. Sulfonated fluorinated multi-block copolymer hybrid containing sulfonated (poly ether ether ketone) and graphene oxide: A ternary hybrid membrane architecture for electrolyte applications in proton exchange membrane fuel cells. *Journal of energy chemistry,* 27**,** 1247-1260.

KUMAR, P. V., SHAMEEM, U., KOLLU, P., KALYANI, R. & PAMMI, S. 2015. Green synthesis of copper oxide nanoparticles using Aloe vera leaf extract and its antibacterial activity against fish bacterial pathogens. *BioNanoScience,* 5**,** 135-139.

KUMAR, S. P., BALAJI, D. & MANDLIMATH, T. R. 2023. Characterization of flexible ceramics. *Advanced Flexible Ceramics.* Elsevier.

KUMARI, S. C., DHAND, V. & PADMA, P. N. 2021. Green synthesis of metallic nanoparticles: a review. *Nanomaterials***,** 259-281.

LAI, W. H., SU, Y. H., TEOH, L. G. & HON, M. H. 2008. Commercial and natural dyes as photosensitizers for a water-based dye-sensitized solar cell loaded with gold nanoparticles. *Journal of Photochemistry and Photobiology A: Chemistry,* 195**,** 307-313.

LE PEVELEN, D. 2010. Small molecule X-ray crystallography, theory and workflow. encyclopedia of spectroscopy and spectrometry. Elsevier.

LI, Y.-Y., LI, C.-T., YEH, M.-H., HUANG, K.-C., CHEN, P.-W., VITTAL, R. & HO, K.-C. 2015. Graphite with different structures as catalysts for counter electrodes in dye-sensitized solar cells. *Electrochimica Acta,* 179**,** 211-219.

MAAZA, M., HENINI, M., EZEMA, F., MANIKANDAN, E., KENNEDY, J., BOUZIANE, K., CHAKER, M., GIBAUD, A., HAQUE, A. & NURU, Z. 2022. Peculiar size effects in nanoscaled systems. *Nano-Horizons: Journal of Nanosciences and Nanotechnologies,* 1**,** 36 pages-36 pages.

MARKVART, T. & CASTAÑER, L. 2018. Principles of solar cell operation. *McEvoy's Handbook of Photovoltaics.* Elsevier.

MEHRBAN, N. & BOWEN, J. 2017. Monitoring biomineralization of biomaterials in vivo. *Monitoring and Evaluation of Biomaterials and their Performance In Vivo.* Elsevier.

MEJICA, G. F. C., UNPAPROM, Y. & RAMARAJ, R. 2023. Fabrication and performance evaluation of dye-sensitized solar cell integrated with natural dye from Strobilanthes cusia under different counter-electrode materials. *Applied Nanoscience,* 13**,** 1073-1083.

MINGSUKANG, M. A., BURAIDAH, M. H., AROF, A. K. & DAS, N. 2017. Third-generation-sensitized solar cells. *Nanostructured Solar Cells***,** 1-9.

MISHRA, A., BHATT, N. & BAJPAI, A. 2019. Nanostructured superhydrophobic coatings for solar panel applications. *Nanomaterials-Based Coatings.* Elsevier.

MITZI, D. B., KOSBAR, L. L., MURRAY, C. E., COPEL, M. & AFZALI, A. 2004. High-mobility ultrathin semiconducting films prepared by spin coating. *Nature,* 428**,** 299-303.

MOHAMED, H., THEMA, T. & DHLAMINI, M. 2021. Green synthesis of CuO nanoparticles via Hyphaene thebaica extract and their optical properties. *Materials Today: Proceedings,* 36**,** 591-594.

MORA-SERÓ, I., SALIBA, M. & ZHOU, Y. 2020. Towards the next decade for perovskite solar cells. Wiley Online Library.

MORAM, M. & VICKERS, M. 2009. X-ray diffraction of III-nitrides. *Reports on progress in physics,* 72**,** 036502.

MORKA, J., OTTIH, I. & UMEOKWONNA, N. 2022. Growth and Characterization of Dye-Sensitized Solar Cells using Dyes from Mangifera Indica, Manihot Esculenta and Hibiscus Sabdariffa Leaves by Sol-Gel Technique. *Journal of Applied Sciences and Environmental Management,* 26**,** 1785-1789.

MUKHOKOSI, E. P., KRUPANIDHI, S. B. & NANDA, K. K. 2017. Band gap engineering of hexagonal SnSe2 nanostructured thin films for infra-red photodetection. *Scientific reports,* 7**,** 15215.

MUNANDAR, M., HAKIM, A., PUSPITADINDHA, H., ANDIYANI, S. & NUROSYID, F. The effect of mixing Chlorophyll-Antocyanin as a natural source dye on the efficiency of dye-sensitized solar cell (DSSC). Journal of Physics: Conference Series, 2022. IOP Publishing, 012042.

MURAKAMI, T. N., ITO, S., WANG, Q., NAZEERUDDIN, M. K., BESSHO, T., CESAR, I., LISKA, P., HUMPHRY-BAKER, R., COMTE, P. & PÉCHY, P. 2006. Highly

efficient dye-sensitized solar cells based on carbon black counter electrodes. *Journal of the Electrochemical Society,* 153**,** A2255.

NABIYOUNI, G., SAHRAEI, R., TOGHIANY, M., ARA, M. M. & HEDAYATI, K. 2011. Preparation and characterization of nanostructured ZnS thin films grown on glass and N-type Si substrates using a new chemical bath deposition technique. *Rev. Adv. Mater. Sci,* 27**,** 52-57.

NAZEERUDDIN, M. K., BARANOFF, E. & GRÄTZEL, M. 2011. Dye-sensitized solar cells: A brief overview. *Solar energy,* 85**,** 1172-1178.

O'REGAN, B. & GRÄTZEL, M. 1991. A low-cost, high-efficiency solar cell based on dye-sensitized colloidal TiO2 films. *nature,* 353**,** 737-740.

PALUPI, E. K., NAZOPATUL, P., UMAM, R., ANDRIANA, B. B., SATO, H. & ALATAS, H. Molecular functional group and optical analysis on chlorophyll of green choy sum and cassava leaves extracts. IOP Conference Series: Earth and Environmental Science, 2020. IOP Publishing, 012030.

PANDIKUMAR, A., JOTHIVENKATACHALAM, K. & BHOJANAA, K. B. 2019. *Interfacial Engineering in Functional Materials for Dye-Sensitized Solar Cells*, John Wiley & Sons.

PAPAGEORGIOU, N., MAIER, W. & GRÄTZEL, M. 1997. An iodine/triiodide reduction electrocatalyst for aqueous and organic media. *Journal of the electrochemical Society,* 144**,** 876.

PARVEEN, K., BANSE, V. & LEDWANI, L. Green synthesis of nanoparticles: their advantages and disadvantages. AIP conference proceedings, 2016. AIP Publishing LLC, 020048.

PRATIWI, D., NUROSYID, F., SUPRIYANTO, A. & SURYANA, R. Optical properties of natural dyes on the dye-sensitized solar cells (DSSC) performance. Journal of Physics: Conference Series, 2016. IOP Publishing, 012007.

PUEYO, A. & MAESTRE, M. 2019. Linking energy access, gender and poverty: A review of the literature on productive uses of energy. *Energy Research & Social Science,* 53**,** 170-181.

RAO, S. S., GOPI, C. V., KIM, S.-K., SON, M.-K., JEONG, M.-S., SAVARIRAJ, A. D., PRABAKAR, K. & KIM, H.-J. 2014. Cobalt sulfide thin film as an efficient counter electrode for dye-sensitized solar cells. *Electrochimica Acta,* 133**,** 174-179.

REPINS, I., CONTRERAS, M. A., EGAAS, B., DEHART, C., SCHARF, J., PERKINS, C. L., TO, B. & NOUFI, R. 2008. 19· 9%-efficient ZnO/CdS/CuInGaSe2 solar cell with 81· 2% fill factor. *Progress in Photovoltaics: Research and applications,* 16**,** 235-239.

ROSTAMABADI, H., FALSAFI, S. R. & JAFARI, S. M. 2020. Transmission electron microscopy (TEM) of nanoencapsulated food ingredients. *Characterization of nanoencapsulated food ingredients.* Elsevier.

ROY, R., CHOUDHARY, V., PATRA, M. & PANDYA, A. 2006. Effect of annealing temperature on the electrical and optical properties of nanocrystalline selenium thin films. *Journal of optoelectronics and advanced materials,* 8**,** 1352.

SAGADEVAN, S., PAL, K. & CHOWDHURY, Z. Z. 2017. Fabrication of CuO nanoparticles for structural, optical and dielectric analysis using chemical precipitation method. *Journal of Materials Science: Materials in Electronics,* 28**,** 12591-12597.

SHARMA, J. K., AKHTAR, M. S., AMEEN, S., SRIVASTAVA, P. & SINGH, G. 2015. Green synthesis of CuO nanoparticles with leaf extract of Calotropis gigantea and its dye-sensitized solar cells applications. *Journal of Alloys and Compounds,* 632**,** 321-325.

SHASHANKA, R., ESGIN, H., YILMAZ, V. M. & CAGLAR, Y. 2020. Fabrication and characterization of green synthesized ZnO nanoparticle based dye-sensitized solar cells. *Journal of Science: Advanced Materials and Devices,* 5**,** 185-191.

SINGH, D., KUNDU, V. S. & MAAN, A. 2016. Structural, morphological and gas sensing study of zinc doped tin oxide nanoparticles synthesized via hydrothermal technique. *Journal of Molecular Structure,* 1115**,** 250-257.

SINTON, R. A. & CUEVAS, A. A quasi-steady-state open-circuit voltage method for solar cell characterization. Proceedings of the 16th European photovoltaic solar energy conference, 2000. 4.

SNAITH, H. J., MOULE, A. J., KLEIN, C., MEERHOLZ, K., FRIEND, R. H. & GRÄTZEL, M. 2007. Efficiency enhancements in solid-state hybrid solar cells via reduced charge recombination and increased light capture. *Nano Letters,* 7**,** 3372-3376.

SONG, C., WANG, S., DONG, W., FANG, X., SHAO, J., ZHU, J. & PAN, X. 2016. Hydrothermal synthesis of iron pyrite (FeS2) as efficient counter electrodes for dye-sensitized solar cells. *Solar Energy,* 133**,** 429-436.

TITUS, D., SAMUEL, E. & ROOPAN, S. 2019. Green Synthesis, Characterization and Applications of Nanoparticles-Chapter 12. *Micro and Nano Technologies***,** 303-319.

TRIBUTSCH, H. 1972. Reaction of excited chlorophyll molecules at electrodes and in photosynthesis. *Photochemistry and Photobiology,* 16**,** 261-269.

TRIHUTOMO, P., SOEPARMAN, S., WIDHIYANURIYAWAN, D. & YULIATI, L. 2019. Performance improvement of dye-sensitized solar cell-(DSSC-) based natural dyes by clathrin protein. *International Journal of Photoenergy,* 2019**,** 1-9.

UL-HAMID, A. 2018. *A beginners' guide to scanning electron microscopy*, Springer.

UNDAVALLI, V. K., LING, C. & KHANDELWAL, B. 2021. Impact of alternative fuels and properties on elastomer compatibility. *Aviation Fuels.* Elsevier.

VIJAYA KUMAR, R., ELGAMIEL, R., DIAMANT, Y., GEDANKEN, A. & NORWIG, J. 2001. Sonochemical preparation and characterization of nanocrystalline copper oxide embedded in poly (vinyl alcohol) and its effect on crystal growth of copper oxide. *Langmuir,* 17**,** 1406-1410.

VISHVESHVAR, K., ARAVIND KRISHNAN, M., HARIBABU, K. & VISHNUPRASAD, S. 2018. Green synthesis of copper oxide nanoparticles using Ixiro coccinea plant leaves and its characterization. *BioNanoScience,* 8**,** 554-558.

WU, C.-S., CHANG, T.-W., TENG, H. & LEE, Y.-L. 2016. High performance carbon black counter electrodes for dye-sensitized solar cells. *Energy,* 115**,** 513-518.

XIAO, Y., HAN, G., LI, Y., LI, M. & CHANG, Y. 2014. High performance of Pt-free dye-sensitized solar cells based on two-step electropolymerized polyaniline counter electrodes. *Journal of Materials Chemistry A,* 2**,** 3452-3460.

XU, H., ZHANG, X., ZHANG, C., LIU, Z., ZHOU, X., PANG, S., CHEN, X., DONG, S., ZHANG, Z. & ZHANG, L. 2012. Nanostructured titanium nitride/PEDOT: PSS composite films as counter electrodes of dye-sensitized solar cells. *ACS applied materials & interfaces,* 4**,** 1087-1092.

YANG, Y., ZHANG, C. & HU, Z. 2013. Impact of metallic and metal oxide nanoparticles on wastewater treatment and anaerobic digestion. *Environmental Science: Processes & Impacts,* 15**,** 39-48.

YILBAS, B., AL-SHARAFI, A. & ALI, H. 2019. *Self-cleaning of surfaces and water droplet mobility,* Elsevier.

YOHANNES, T. & INGANÄS, O. 1998. Photoelectrochemical studies of the junction between poly [3-(4-octylphenyl) thiophene] and a redox polymer electrolyte. *Solar Energy Materials and Solar Cells,* 51**,** 193-202.

YUN, S., WANG, L., GUO, W. & MA, T. 2012. Non-Pt counter electrode catalysts using tantalum oxide for low-cost dye-sensitized solar cells. *Electrochemistry communications,* 24**,** 69-73.

YUNIATI, Y., ELIM, P., ALFANAAR, R. & KUSUMA, H. Extraction of anthocyanin pigment from hibiscus sabdariffa l. by ultrasonic-assisted extraction. IOP Conference Series: Materials Science and Engineering, 2021. IOP Publishing, 012032.

ZHAO, W., ZHU, X., BI, H., CUI, H., SUN, S. & HUANG, F. 2013. Novel two-step synthesis of NiS nanoplatelet arrays as efficient counter electrodes for dye-sensitized solar cells. *Journal of power sources,* 242**,** 28-32.

ZHENG, X., XU, C., TOMOKIYO, Y., TANAKA, E., YAMADA, H. & SOEJIMA, Y. 2000. Observation of charge stripes in cupric oxide. *Physical Review Letters,* 85**,** 5170.

ZHOU, C., HU, H., YANG, Y., CHEN, B., ZHANG, J., WU, S., XU, S., XIONG, X., HAN, H. & ZHAO, X. 2008. Effect of thickness on structural, electrical, and electrochemical properties of platinum/titanium bilayer counterelectrode. *Journal of Applied Physics,* 104**,** 034910.

ZHOU, W., APKARIAN, R., WANG, Z. L. & JOY, D. 2006. Fundamentals of scanning electron microscopy (SEM). *Scanning microscopy for nanotechnology.* Springer.

ZHU, Y., MIMURA, K. & ISSHIKI, M. 2003. Influence of small amounts of impurities on copper oxidation at 600–1050° C. *Oxidation of metals,* 59**,** 575-590.

APPENDICES

APPENDIX A: Raw data

All the raw data is available with the Principal Investigator on request.

APPENDIX B: Permission to re-use figures from other publications. Figures 2.1, 2.3, 2.4, 2.5, 2.6, 2.7, 2.8, 2.9 and 2.10 were reproduced with permission from the authors as indicated in the sub sections of appendix B.

Appendix B.1: Permission to re-use Figure 2.1.

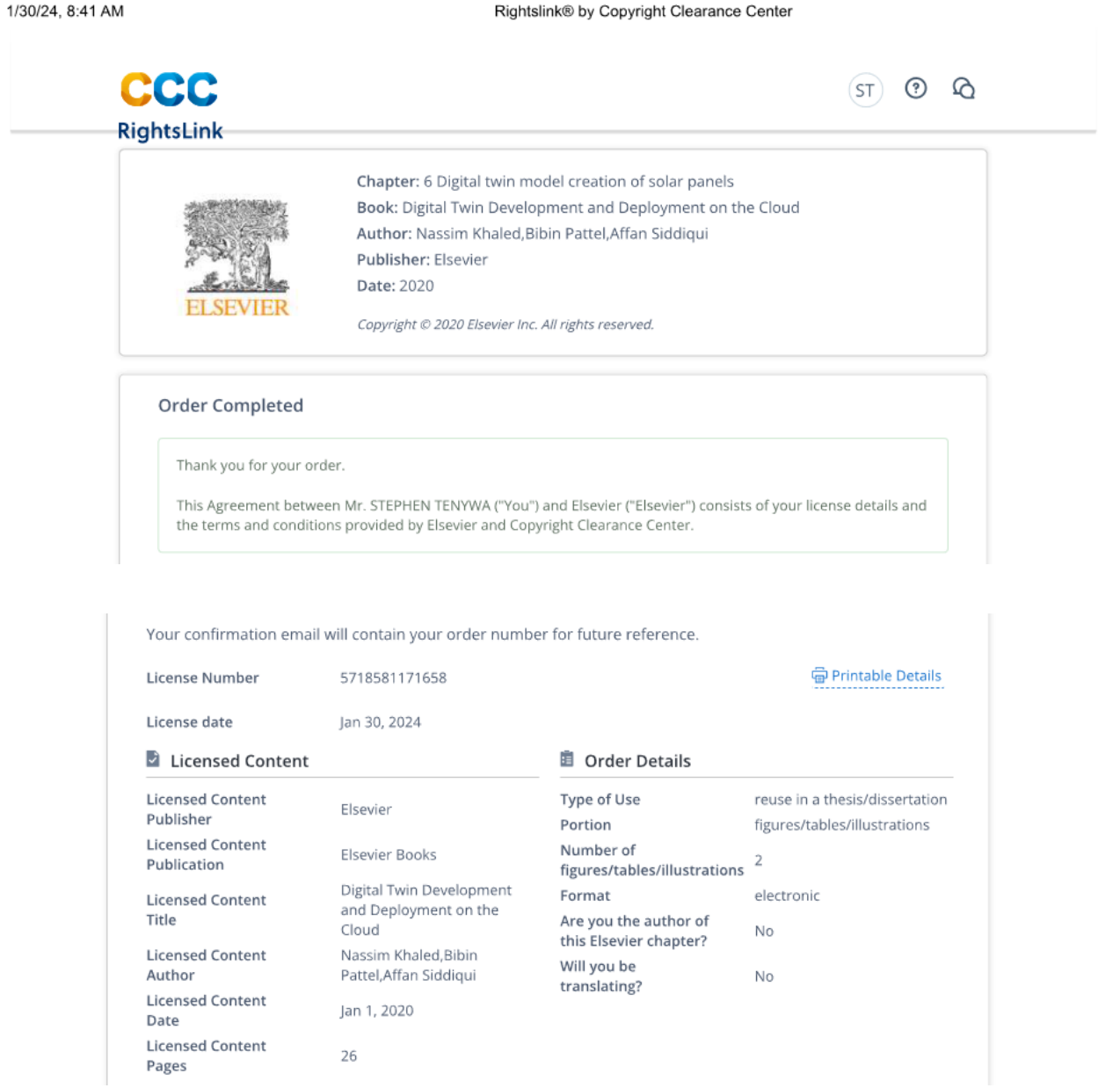

1/30/24, 8:41 AM Rightslink® by Copyright Clearance Center

CCC RightsLink

ST

ELSEVIER

Chapter: 6 Digital twin model creation of solar panels
Book: Digital Twin Development and Deployment on the Cloud
Author: Nassim Khaled,Bibin Pattel,Affan Siddiqui
Publisher: Elsevier
Date: 2020

Copyright © 2020 Elsevier Inc. All rights reserved.

Order Completed

Thank you for your order.

This Agreement between Mr. STEPHEN TENYWA ("You") and Elsevier ("Elsevier") consists of your license details and the terms and conditions provided by Elsevier and Copyright Clearance Center.

Your confirmation email will contain your order number for future reference.

License Number	5718581171658
License date	Jan 30, 2024

Printable Details

Licensed Content

Licensed Content Publisher	Elsevier
Licensed Content Publication	Elsevier Books
Licensed Content Title	Digital Twin Development and Deployment on the Cloud
Licensed Content Author	Nassim Khaled,Bibin Pattel,Affan Siddiqui
Licensed Content Date	Jan 1, 2020
Licensed Content Pages	26

Order Details

Type of Use	reuse in a thesis/dissertation
Portion	figures/tables/illustrations
Number of figures/tables/illustrations	2
Format	electronic
Are you the author of this Elsevier chapter?	No
Will you be translating?	No

About Your Work

Title of new work	GREEN SYNTHESIS OF COPPER OXIDE NANOPARTICLES FROM Cucurbita maxima DYE EXTRACT: A PLATINUM FREE COUNTER ELECTRODE FOR DYE SENSITIZED SOLAR CELLS
Institution name	KYAMBOGO UNIVERSITY
Expected presentation date	Jan 2024

Additional Data

Order reference number	https://doi.org/10.1016/B978-0-12-821631-6.00006-2
Portions	2

Requestor Location

Mr. STEPHEN TENYWA KYAMBOGO

Requestor Location

KAMPALA, CENTRAL 0000
Uganda
Attn: Mr. STEPHEN TENYWA

Tax Details

Publisher Tax ID	GB 494 6272 12

Total: 0.00 USD

CLOSE WINDOW ORDER MORE

Appendix B.2: Permission to re-use Figure 2.3.

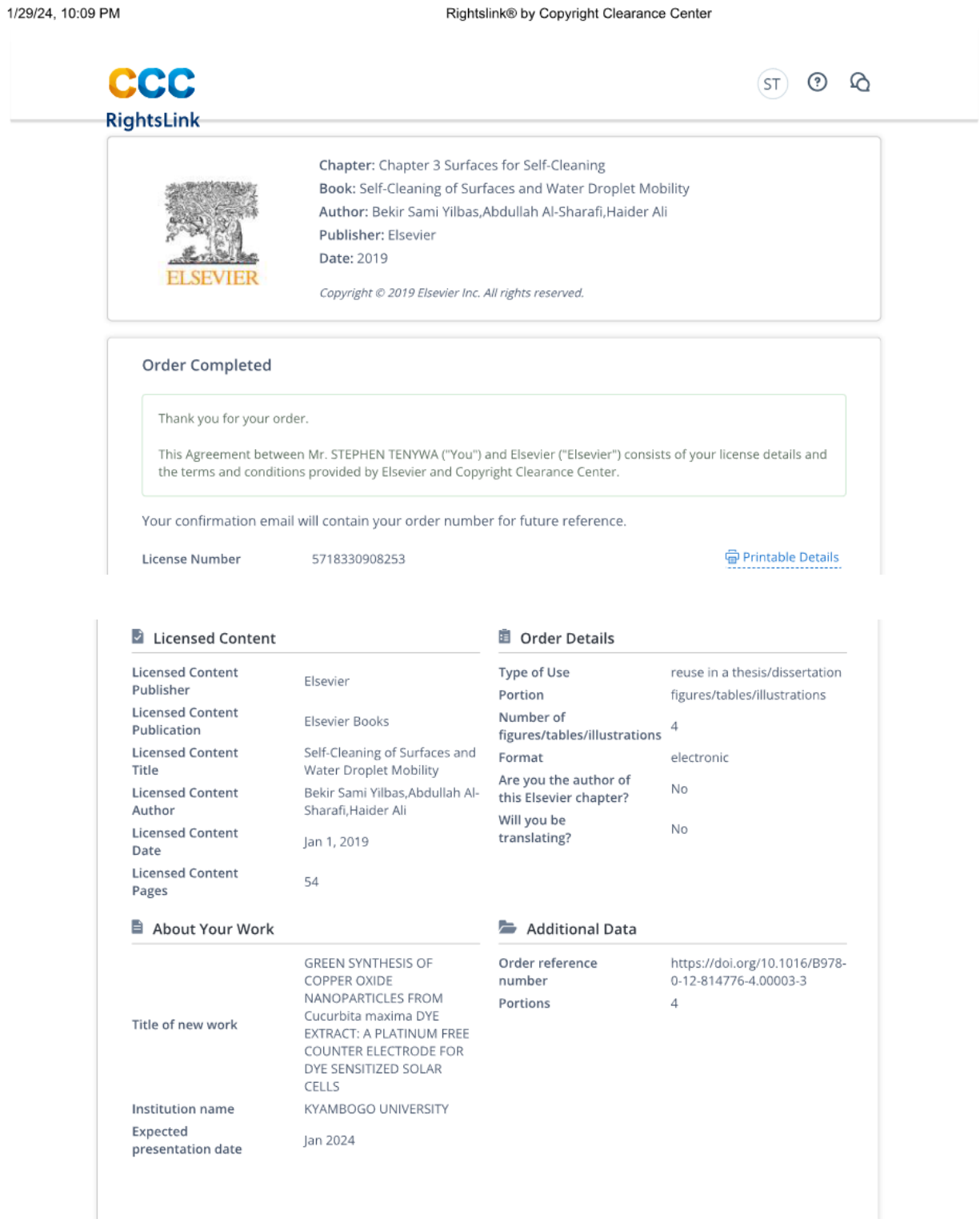

1/29/24, 10:09 PM Rightslink® by Copyright Clearance Center

RightsLink

Chapter: Chapter 3 Surfaces for Self-Cleaning
Book: Self-Cleaning of Surfaces and Water Droplet Mobility
Author: Bekir Sami Yilbas,Abdullah Al-Sharafi,Haider Ali
Publisher: Elsevier
Date: 2019

Copyright © 2019 Elsevier Inc. All rights reserved.

Order Completed

Thank you for your order.

This Agreement between Mr. STEPHEN TENYWA ("You") and Elsevier ("Elsevier") consists of your license details and the terms and conditions provided by Elsevier and Copyright Clearance Center.

Your confirmation email will contain your order number for future reference.

License Number 5718330908253 Printable Details

Licensed Content

Licensed Content Publisher	Elsevier
Licensed Content Publication	Elsevier Books
Licensed Content Title	Self-Cleaning of Surfaces and Water Droplet Mobility
Licensed Content Author	Bekir Sami Yilbas,Abdullah Al-Sharafi,Haider Ali
Licensed Content Date	Jan 1, 2019
Licensed Content Pages	54

Order Details

Type of Use	reuse in a thesis/dissertation
Portion	figures/tables/illustrations
Number of figures/tables/illustrations	4
Format	electronic
Are you the author of this Elsevier chapter?	No
Will you be translating?	No

About Your Work

Title of new work	GREEN SYNTHESIS OF COPPER OXIDE NANOPARTICLES FROM Cucurbita maxima DYE EXTRACT: A PLATINUM FREE COUNTER ELECTRODE FOR DYE SENSITIZED SOLAR CELLS
Institution name	KYAMBOGO UNIVERSITY
Expected presentation date	Jan 2024

Additional Data

Order reference number	https://doi.org/10.1016/B978-0-12-814776-4.00003-3
Portions	4

Appendix B.3: Permission to re-use Figure 2.4.

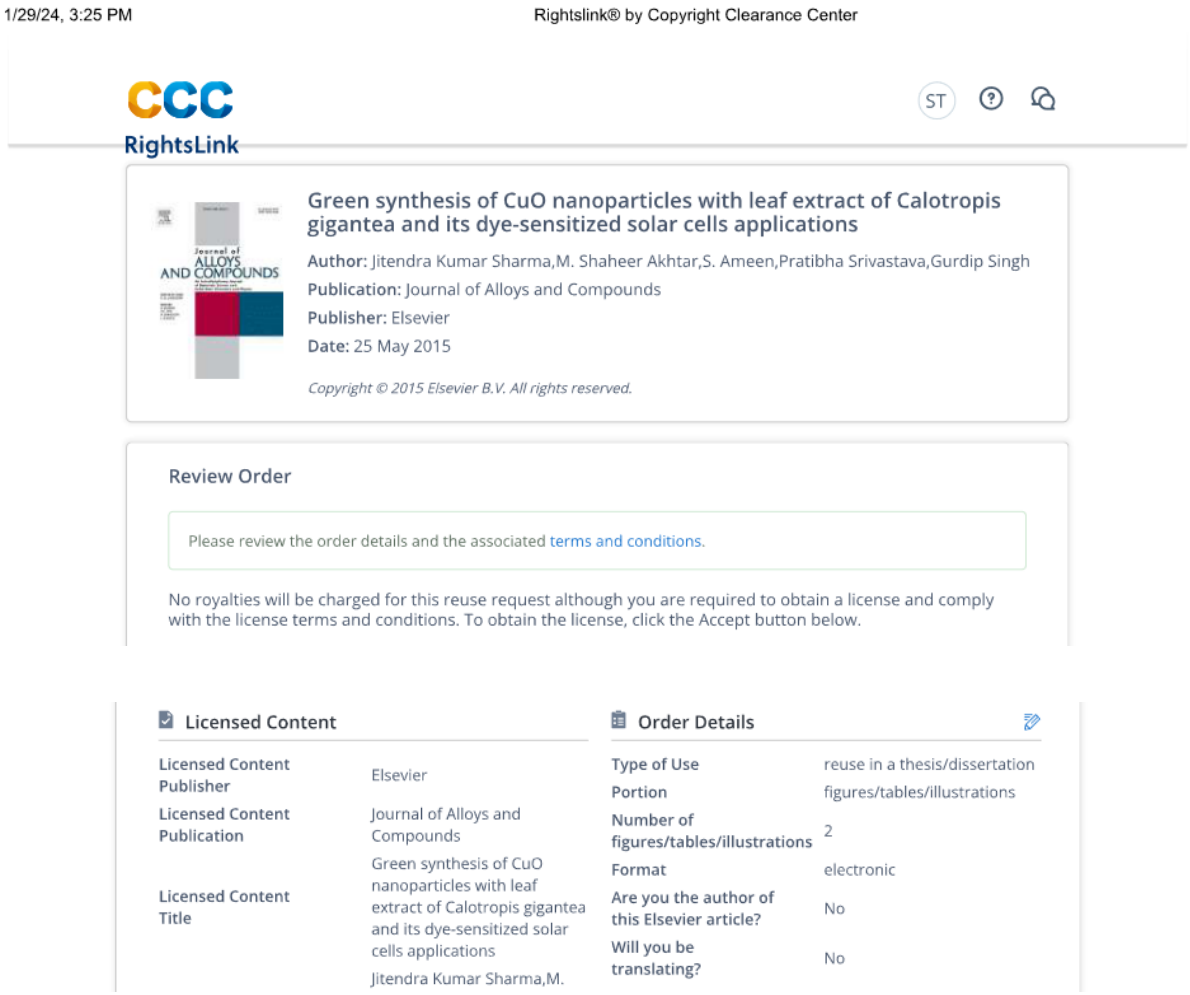

	Jitendra Kumar Sharma,M. Shaheer Akhtar,S. Ameen,Pratibha Srivastava,Gurdip Singh	translating?	
Licensed Content Author			
Licensed Content Date	25 May 2015		
Licensed Content Volume	632		
Licensed Content Issue	n/a		
Licensed Content Pages	5		

About Your Work

Title of new work	GREEN SYNTHESIS OF COPPER OXIDE NANOPARTICLES FROM Cucurbita maxima DYE EXTRACT: A PLATINUM FREE COUNTER ELECTRODE FOR DYE SENSITIZED SOLAR CELLS
Institution name	KYAMBOGO UNIVERSITY
Expected presentation date	Jan 2024

Additional Data

Order reference number	https://doi.org/10.1016/j.jallcom.2015.01.172
Portions	2

Requestor Location

Mr. STEPHEN TENYWA KYAMBOGO

Requestor Location

KAMPALA, CENTRAL 0000
Uganda
Attn: Mr. STEPHEN TENYWA

Tax Details

Publisher Tax ID	GB 494 6272 12

☐ I agree to these terms and conditions.

☐ I understand this license is for reuse only and that no content is provided.

Total: 0.00 USD

BACK DECLINE SAVE QUOTE ACCEPT

Please click accept only once.

Appendix B.4: Permission to re-use Figure 2.5.

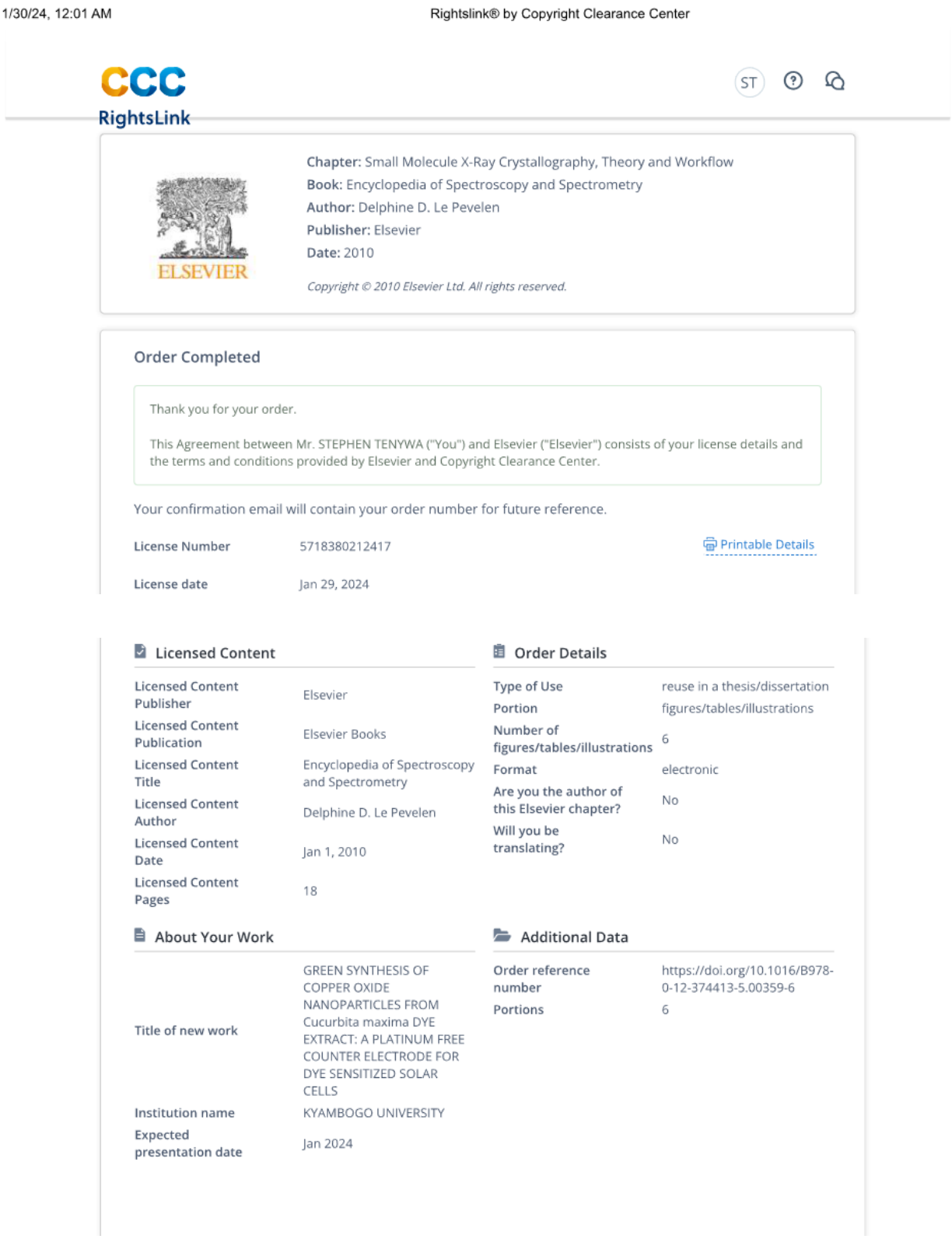

1/30/24, 12:01 AM Rightslink® by Copyright Clearance Center

CCC RightsLink

ST

Chapter: Small Molecule X-Ray Crystallography, Theory and Workflow
Book: Encyclopedia of Spectroscopy and Spectrometry
Author: Delphine D. Le Pevelen
Publisher: Elsevier
Date: 2010

Copyright © 2010 Elsevier Ltd. All rights reserved.

Order Completed

Thank you for your order.

This Agreement between Mr. STEPHEN TENYWA ("You") and Elsevier ("Elsevier") consists of your license details and the terms and conditions provided by Elsevier and Copyright Clearance Center.

Your confirmation email will contain your order number for future reference.

License Number	5718380212417
License date	Jan 29, 2024

Printable Details

Licensed Content

Licensed Content Publisher	Elsevier
Licensed Content Publication	Elsevier Books
Licensed Content Title	Encyclopedia of Spectroscopy and Spectrometry
Licensed Content Author	Delphine D. Le Pevelen
Licensed Content Date	Jan 1, 2010
Licensed Content Pages	18

Order Details

Type of Use	reuse in a thesis/dissertation
Portion	figures/tables/illustrations
Number of figures/tables/illustrations	6
Format	electronic
Are you the author of this Elsevier chapter?	No
Will you be translating?	No

About Your Work

Title of new work	GREEN SYNTHESIS OF COPPER OXIDE NANOPARTICLES FROM Cucurbita maxima DYE EXTRACT: A PLATINUM FREE COUNTER ELECTRODE FOR DYE SENSITIZED SOLAR CELLS
Institution name	KYAMBOGO UNIVERSITY
Expected presentation date	Jan 2024

Additional Data

Order reference number	https://doi.org/10.1016/B978-0-12-374413-5.00359-6
Portions	6

Requestor Location

Mr. STEPHEN TENYWA KYAMBOGO

Requestor Location

KAMPALA, CENTRAL 0000
Uganda
Attn: Mr. STEPHEN TENYWA

Tax Details

Publisher Tax ID GB 494 6272 12

Total: 0.00 USD

CLOSE WINDOW ORDER MORE

Appendix B.5: Permission to re-use Figure 2.6.

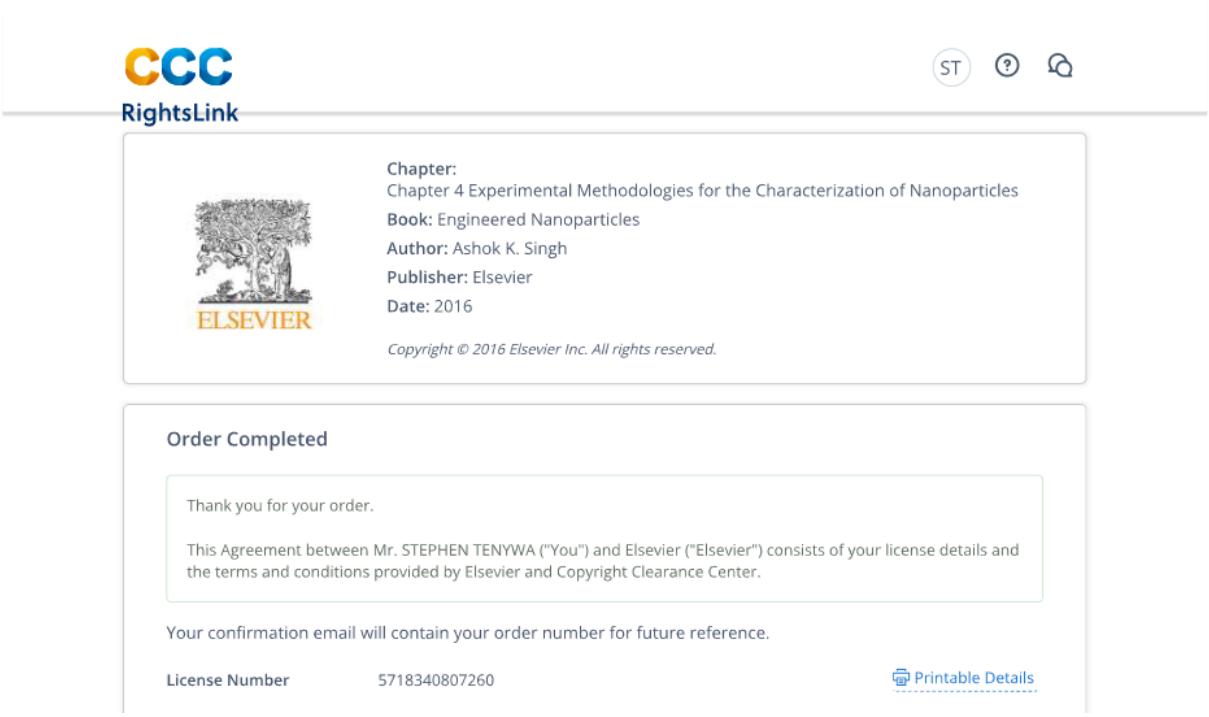

RightsLink

ST

ELSEVIER

Chapter:
Chapter 4 Experimental Methodologies for the Characterization of Nanoparticles
Book: Engineered Nanoparticles
Author: Ashok K. Singh
Publisher: Elsevier
Date: 2016

Order Completed

Thank you for your order.

This Agreement between Mr. STEPHEN TENYWA ("You") and Elsevier ("Elsevier") consists of your license details and the terms and conditions provided by Elsevier and Copyright Clearance Center.

Your confirmation email will contain your order number for future reference.

License Number 5718340807260 Printable Details

Licensed Content

Licensed Content Publisher	Elsevier
Licensed Content Publication	Elsevier Books
Licensed Content Title	Engineered Nanoparticles
Licensed Content Author	Ashok K. Singh
Licensed Content Date	Jan 1, 2016
Licensed Content Pages	46

Order Details

Type of Use	reuse in a thesis/dissertation
Portion	figures/tables/illustrations
Number of figures/tables/illustrations	17
Format	electronic
Are you the author of this Elsevier chapter?	No
Will you be translating?	No

About Your Work

Title of new work	GREEN SYNTHESIS OF COPPER OXIDE NANOPARTICLES FROM Cucurbita maxima DYE EXTRACT: A PLATINUM FREE COUNTER ELECTRODE FOR DYE SENSITIZED SOLAR CELLS
Institution name	KYAMBOGO UNIVERSITY
Expected presentation date	Jan 2024

Additional Data

Order reference number	https://doi.org/10.1016/B978-0-12-801406-6.00004-2
Portions	17

Requestor Location

Mr. STEPHEN TENYWA KYAMBOGO

Requestor Location

KAMPALA, CENTRAL 0000
Uganda
Attn: Mr. STEPHEN TENYWA

Tax Details

Publisher Tax ID	GB 494 6272 12

Total: 0.00 USD

CLOSE WINDOW ORDER MORE

Appendix B.6: Permission to re-use Figure 2.7.

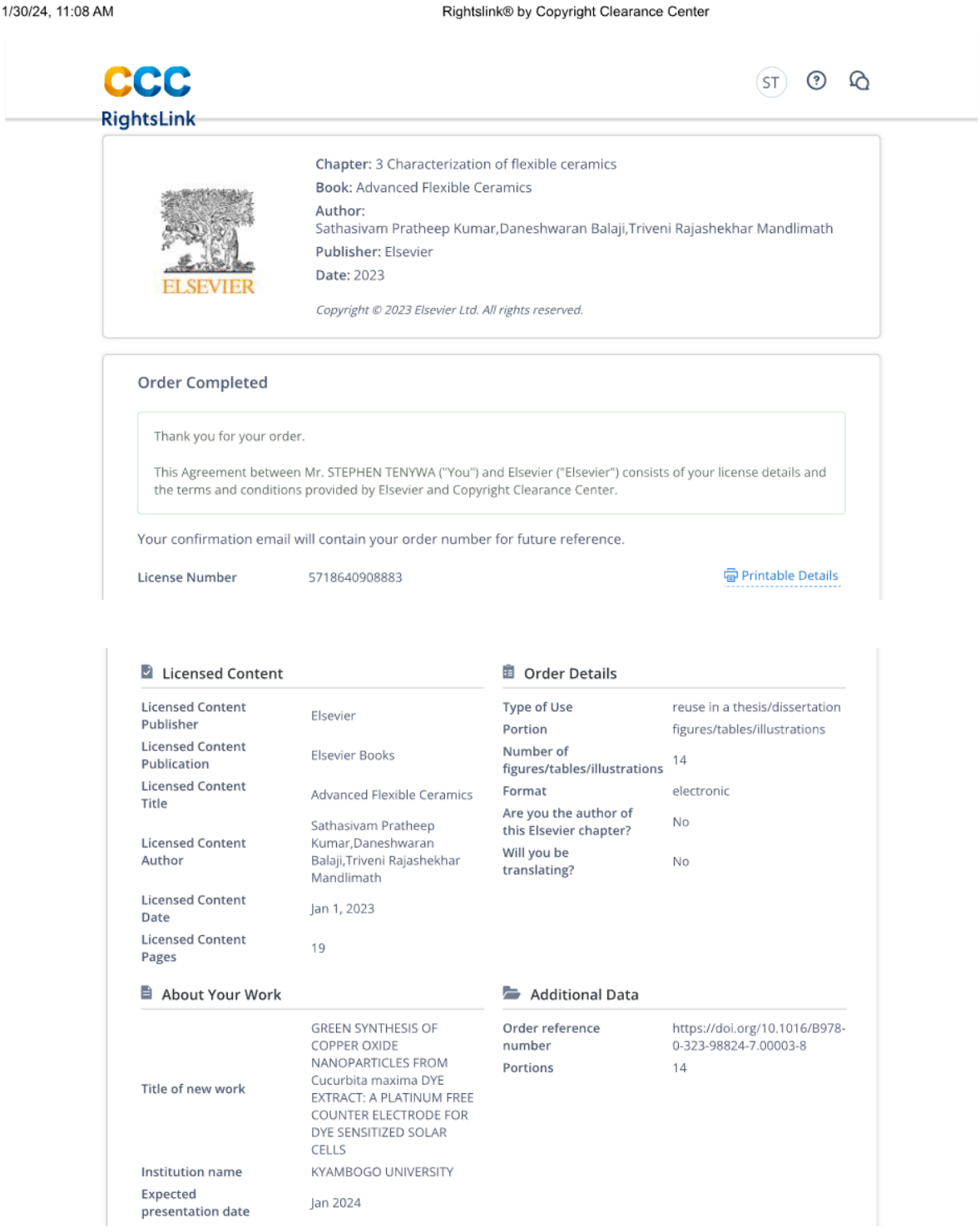

1/30/24, 11:08 AM Rightslink® by Copyright Clearance Center

CCC RightsLink

ST

Chapter: 3 Characterization of flexible ceramics
Book: Advanced Flexible Ceramics
Author: Sathasivam Pratheep Kumar,Daneshwaran Balaji,Triveni Rajashekhar Mandlimath
Publisher: Elsevier
Date: 2023

Copyright © 2023 Elsevier Ltd. All rights reserved.

Order Completed

Thank you for your order.

This Agreement between Mr. STEPHEN TENYWA ("You") and Elsevier ("Elsevier") consists of your license details and the terms and conditions provided by Elsevier and Copyright Clearance Center.

Your confirmation email will contain your order number for future reference.

License Number 5718640908883 Printable Details

Licensed Content

Licensed Content Publisher	Elsevier
Licensed Content Publication	Elsevier Books
Licensed Content Title	Advanced Flexible Ceramics
Licensed Content Author	Sathasivam Pratheep Kumar,Daneshwaran Balaji,Triveni Rajashekhar Mandlimath
Licensed Content Date	Jan 1, 2023
Licensed Content Pages	19

Order Details

Type of Use	reuse in a thesis/dissertation
Portion	figures/tables/illustrations
Number of figures/tables/illustrations	14
Format	electronic
Are you the author of this Elsevier chapter?	No
Will you be translating?	No

About Your Work

Title of new work	GREEN SYNTHESIS OF COPPER OXIDE NANOPARTICLES FROM Cucurbita maxima DYE EXTRACT: A PLATINUM FREE COUNTER ELECTRODE FOR DYE SENSITIZED SOLAR CELLS
Institution name	KYAMBOGO UNIVERSITY
Expected presentation date	Jan 2024

Additional Data

Order reference number	https://doi.org/10.1016/B978-0-323-98824-7.00003-8
Portions	14

Appendix B.7: Permission to re-use Figure 2.8.

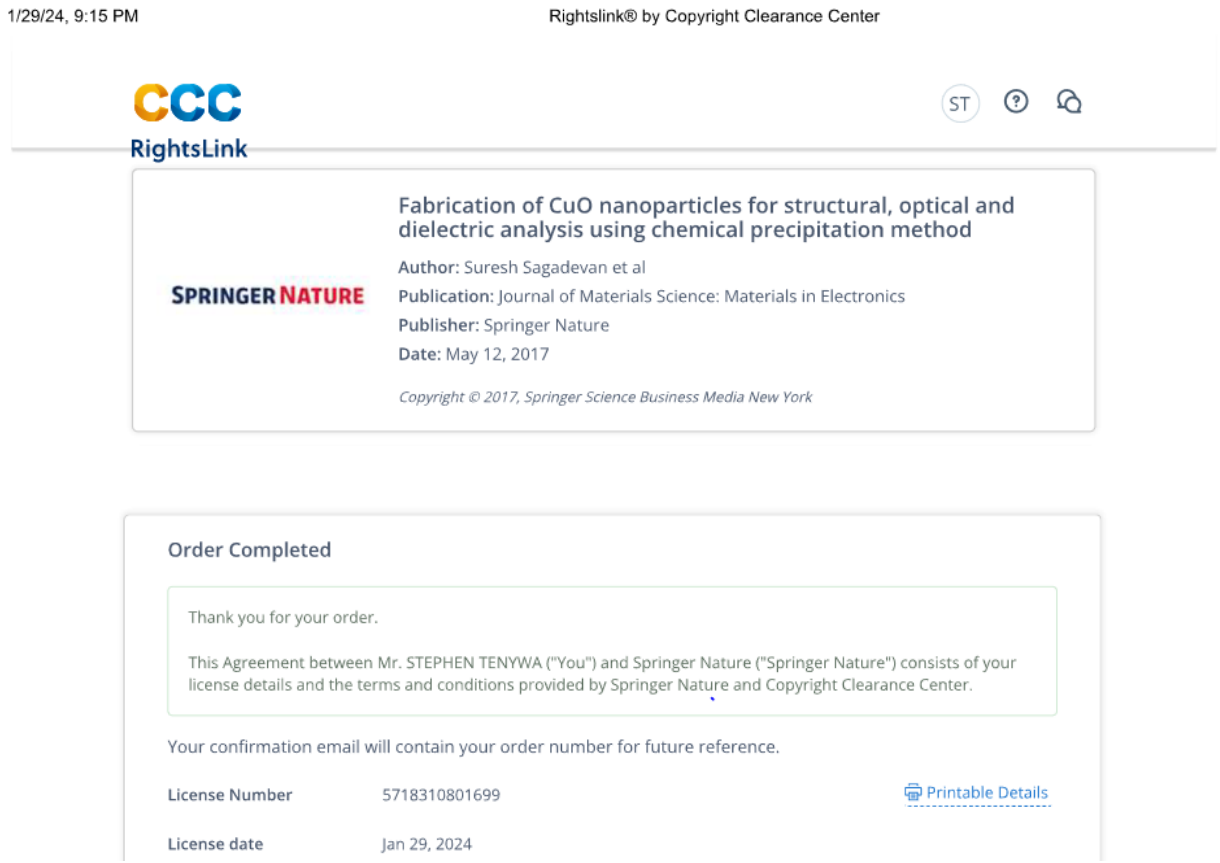

Licensed Content

Licensed Content Publisher	Springer Nature
Licensed Content Publication	Journal of Materials Science: Materials in Electronics
Licensed Content Title	Fabrication of CuO nanoparticles for structural, optical and dielectric analysis using chemical precipitation method
Licensed Content Author	Suresh Sagadevan et al
Licensed Content Date	May 12, 2017

Order Details

Type of Use	Thesis/Dissertation
Requestor type	academic/university or research institute
Format	electronic
Portion	figures/tables/illustrations
Number of figures/tables/illustrations	5
Will you be translating?	no
Circulation/distribution	1 - 29
Author of this Springer Nature content	no

About Your Work

Title of new work	GREEN SYNTHESIS OF COPPER OXIDE NANOPARTICLES FROM Cucurbita maxima DYE EXTRACT: A PLATINUM FREE COUNTER ELECTRODE FOR DYE SENSITIZED SOLAR CELLS
Institution name	KYAMBOGO UNIVERSITY
Expected presentation date	Jan 2024

Additional Data

Order reference number	https://link.springer.com/article/10.1007/s10854-017-7083-3
Portions	5

Requestor Location

Mr. STEPHEN TENYWA KYAMBOGO

Requestor Location

KAMPALA, CENTRAL 0000
Uganda
Attn: Mr. STEPHEN TENYWA

Tax Details

Total: 0.00 USD

CLOSE WINDOW ORDER MORE

Appendix B.8: Permission to re-use Figure 2.9.

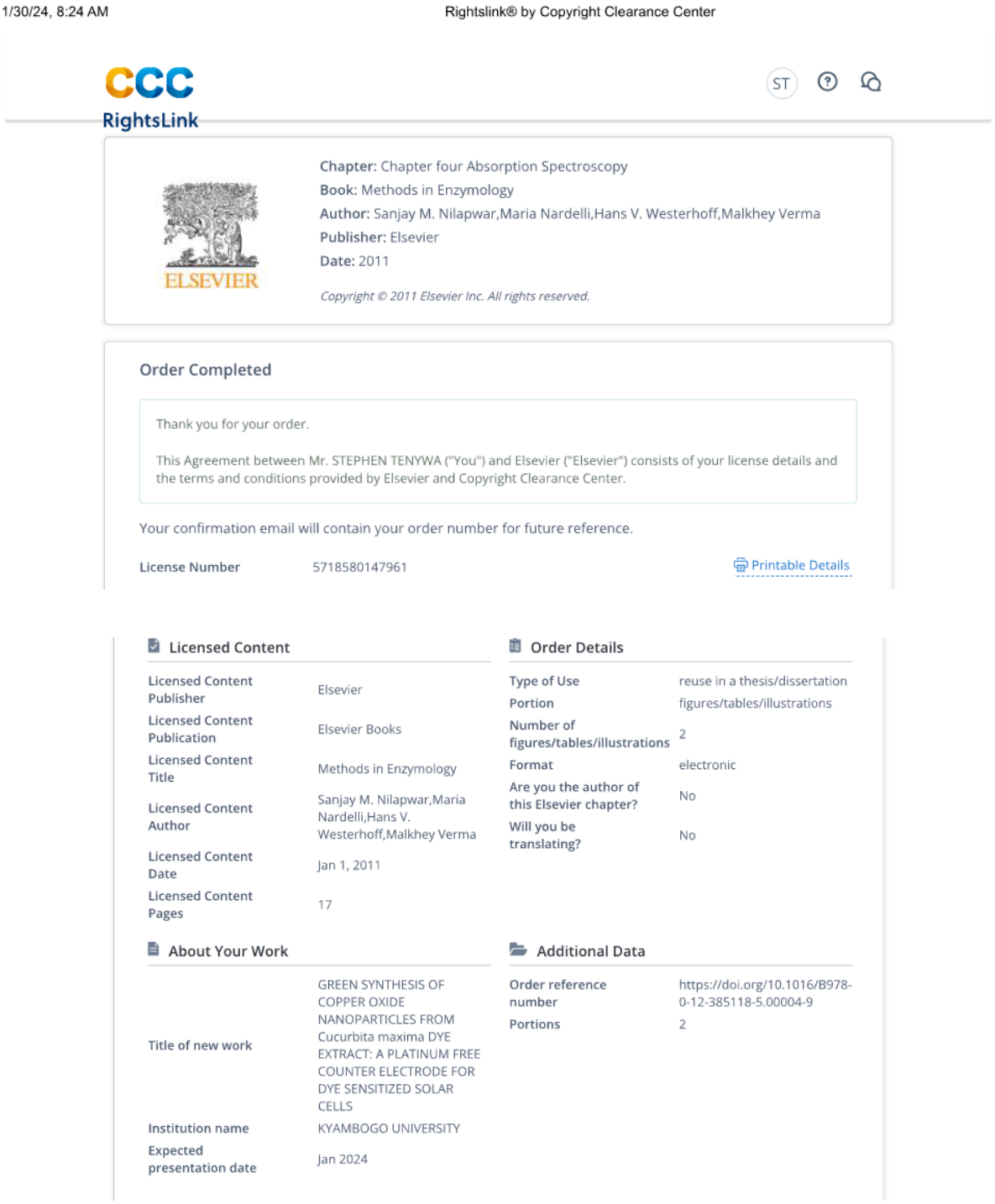

1/30/24, 8:24 AM Rightslink® by Copyright Clearance Center

CCC RightsLink

ST

Chapter: Chapter four Absorption Spectroscopy
Book: Methods in Enzymology
Author: Sanjay M. Nilapwar,Maria Nardelli,Hans V. Westerhoff,Malkhey Verma
Publisher: Elsevier
Date: 2011

Copyright © 2011 Elsevier Inc. All rights reserved.

Order Completed

Thank you for your order.

This Agreement between Mr. STEPHEN TENYWA ("You") and Elsevier ("Elsevier") consists of your license details and the terms and conditions provided by Elsevier and Copyright Clearance Center.

Your confirmation email will contain your order number for future reference.

License Number 5718580147961 Printable Details

Licensed Content

Licensed Content Publisher	Elsevier
Licensed Content Publication	Elsevier Books
Licensed Content Title	Methods in Enzymology
Licensed Content Author	Sanjay M. Nilapwar,Maria Nardelli,Hans V. Westerhoff,Malkhey Verma
Licensed Content Date	Jan 1, 2011
Licensed Content Pages	17

Order Details

Type of Use	reuse in a thesis/dissertation
Portion	figures/tables/illustrations
Number of figures/tables/illustrations	2
Format	electronic
Are you the author of this Elsevier chapter?	No
Will you be translating?	No

About Your Work

Title of new work	GREEN SYNTHESIS OF COPPER OXIDE NANOPARTICLES FROM Cucurbita maxima DYE EXTRACT: A PLATINUM FREE COUNTER ELECTRODE FOR DYE SENSITIZED SOLAR CELLS
Institution name	KYAMBOGO UNIVERSITY
Expected presentation date	Jan 2024

Additional Data

Order reference number	https://doi.org/10.1016/B978-0-12-385118-5.00004-9
Portions	2

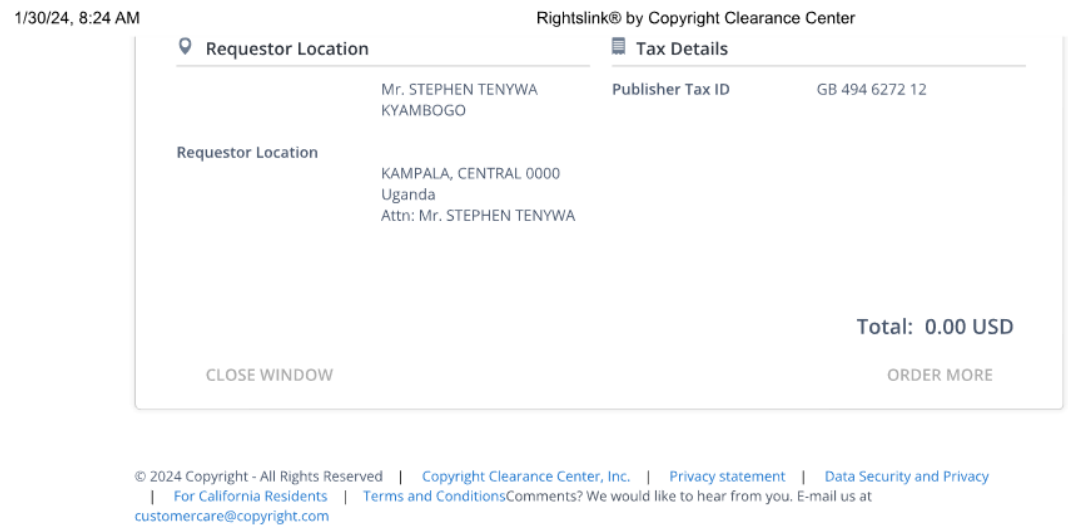

Appendix B.9: Permission to re-use Figure 2.10.

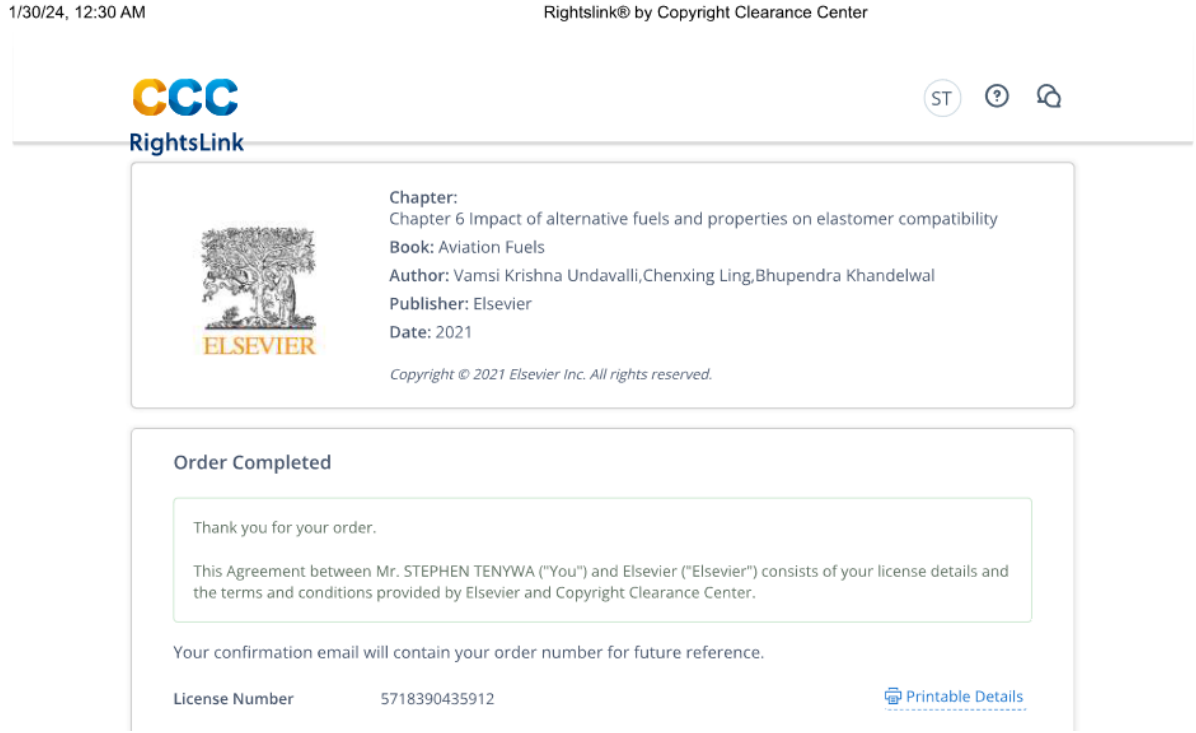

Licensed Content

Licensed Content Publisher	Elsevier
Licensed Content Publication	Elsevier Books
Licensed Content Title	Aviation Fuels
Licensed Content Author	Vamsi Krishna Undavalli,Chenxing Ling,Bhupendra Khandelwal
Licensed Content Date	Jan 1, 2021
Licensed Content Pages	20

Order Details

Type of Use	reuse in a thesis/dissertation
Portion	figures/tables/illustrations
Number of figures/tables/illustrations	6
Format	electronic
Are you the author of this Elsevier chapter?	No
Will you be translating?	No

About Your Work

Title of new work	GREEN SYNTHESIS OF COPPER OXIDE NANOPARTICLES FROM Cucurbita maxima DYE EXTRACT: A PLATINUM FREE COUNTER ELECTRODE FOR DYE SENSITIZED SOLAR CELLS
Institution name	KYAMBOGO UNIVERSITY
Expected presentation date	Jan 2024

Additional Data

Order reference number	https://doi.org/10.1016/B978-0-12-818314-4.00001-7
Portions	6

Requestor Location

	Mr. STEPHEN TENYWA KYAMBOGO
Requestor Location	KAMPALA, CENTRAL 0000 Uganda Attn: Mr. STEPHEN TENYWA

Tax Details

Publisher Tax ID	GB 494 6272 12

Total: 0.00 USD

CLOSE WINDOW ORDER MORE